NASA TECHNICAL NOTE

NASA TN D-5608

c. 1

NASA TN D-5608

AERODYNAMICS OF MARS ENTRY PROBE-LANDER CONFIGURATIONS AT A MACH NUMBER OF 10

by Robert I. Sammonds

Ames Research Center
Moffett Field, Calif.

NATIONAL AERONAUTICS AND SPACE ADMINISTRATION • WASHINGTON, D. C. • JANUARY 1970

1. Report No. NASA TN D-5608	2. Government Accession No.	3. Recipient's Catalog No.
4. Title and Subtitle AERODYNAMICS OF MARS ENTRY PROBE-LANDER CONFIGURATIONS AT A MACH NUMBER OF 10		5. Report Date January 1970 6. Performing Organization Code
7. Author(s) Robert I. Sammonds		8. Performing Organization Report No. A-3334
9. Performing Organization Name and Address NASA Ames Research Center Moffett Field, California 94035		10. Work Unit No. 124-07-02-35-00-21 11. Contract or Grant No.
12. Sponsoring Agency Name and Address National Aeronautics and Space Administration Washington D. C. 20546		13. Type of Report and Period Covered Technical Note 14. Sponsoring Agency Code

15. Supplementary Notes

16. Abstract

Five spherically blunted cones were tested in free flight, in still air, to determine their aerodynamic characteristics. Three of these models, by design, had drag coefficients invariant with angle of attack ($< 15^0$) and lift-curve slopes near zero. Each of these three models was statically stable but the dynamic stability was found to depend on cone half-angle and nose bluntness.

The lift-curve slopes and dynamic stability of the two high-drag bodies, 55^c and 60^0 half-angle blunted cones, were invariant with angle of attack ($<16^0$) and equal in magnitude. These two models were both statically and dynamically stable.

17. Key Words Suggested by Author	18. Distribution Statement
large angle spherically blunted cones atmospheric entry vehicles Mars probe-lander configurations hypersonic aerodynamics of large angle blunted cones blunt cones dynamic stability ballistic range tests	Unclassified - Unlimited

19. Security Classif. (of this report)	20. Security Classif. (of this page)	21. No. of Pages	22. Price*
Unclassified	Unclassified	55	$3.00

*For sale by the Clearinghouse for Federal Scientific and Technical Information
Springfield, Virginia 22151

SYMBOLS

A	reference area, maximum body cross-sectional area
C_D	drag coefficient, $\frac{\text{drag}}{q_\infty A}$
C_L	lift coefficient, $\frac{\text{lift}}{q_\infty A}$
C_{L_d}	body-fixed lift force due to small model asymmetries at $x = 0$
C_{L_r}	resultant lift force due to small model asymmetries, $\sqrt{\left(C_{L_d}\right)^2 + \left(C_{y_d}\right)^2}$
C_{L_α}	lift-curve slope
C_m	pitching-moment coefficient, $\frac{\text{moment}}{q_\infty Ad}$
C_{m_α}	pitching-moment-curve slope (based on an assumed linear pitching-moment curve)
$C_{m_q}+C_{m_{\dot{\alpha}}}$	damping-in-pitch derivative, $\frac{\partial C_m}{\partial (qd/V)} + \frac{\partial C_m}{\partial (\dot{\alpha}d/V)}$
$C_{p_{max}}$	stagnation-point pressure coefficient
C_{y_d}	body-fixed side force due to small model asymmetries at $x = 0$
d	reference diameter, maximum body diameter
I_x	moment of inertia about the roll axis
I_y	moment of inertia about transverse axis through center of gravity
M	Mach number
m	mass of model
q	angular pitching velocity
q_∞	free-stream dynamic pressure
Re	Reynolds number based on free-stream air properties and model reference diameter, d

r	radius of curvature, rounded corners or model apex
V	velocity of the model with respect to the still air
X_{cg}	axial distance from model nose to center-of-gravity position
X_{cp}	axial distance from model nose to center-of-pressure position
x,y,z	earth-fixed axes, also displacements along these axes
α	angle of attack (angle, projected onto the x-z plane, between model longitudinal axis and the stream direction)
α_m	average value of maximum angle-of-attack envelope
α_{min}	average value of minimum angle-of-attack envelope
α_{rms}	root-mean-square resultant angle of attack, $\left(\frac{\int_0^x \alpha_r \, dx}{x}\right)^{1/2}$
α_r	resultant angle of attack, $\sqrt{\alpha^2 + \beta^2}$
α_t	resultant trim angle of attack
β	angle of sideslip (angle, projected onto the x-y plane, between model axis of symmetry and the stream direction)
θ_a	afterbody cone half-angle
θ_c	forebody cone half-angle
ξ	dynamic-stability parameter, $C_D - C_{L_\alpha} + \left(C_{m_q} + C_{m_{\dot{\alpha}}}\right)\left(\frac{d}{\sigma}\right)^2$
ρ	air density
σ	transverse radius of gyration with respect to the center of gravity of the model, $\sqrt{I_y/m}$
$(\dot{})$	first derivative with respect to time

Subscripts

a	afterbody
b	base
c	corner
n	nose
∞	free-stream conditions

AERODYNAMICS OF MARS ENTRY PROBE-LANDER CONFIGURATIONS AT A MACH NUMBER OF 10

By Robert I. Sammonds

Ames Research Center

SUMMARY

An experimental study to determine the aerodynamic characteristics of several configurations intended for use in exploring the atmosphere of Mars has been conducted in free flight, in still air, at a nominal Mach number of 10 and a Reynolds number (based on model diameter) of 300,000. The configurations tested were three spherically blunted axisymmetric cones designed to have a zero lift-curve slope and constant drag at moderate angles of attack and two higher drag blunt cones with half angles of 60° and 55°.

At angles of attack less than 15°, the drag coefficients of all three "zero lift" models were invariant with angle of attack and the lift-curve slopes were near zero. Each of these configurations was statically stable, with the stability decreasing with increasing angle of attack. The dynamic stability of the three "zero lift" models varied from stable to unstable as the combination of cone half-angle and nose bluntness ratio was varied from a cone half-angle of 44.1° and a nose bluntness ratio of 0.33 to a cone half-angle of 27° and a bluntness ratio of 0.95.

The drag coefficient for the 60° high-drag cone was 1.46 or about 4 percent higher than that obtained for the 55° cone. The lift-curve slope and the dynamic stability were the same for these two high-drag models and essentially constant with angle of attack. These two models were statically and dynamically stable in the angle-of-attack range of these tests. However, of the five configurations tested the static stability of only the 60° cone increased with increasing angle of attack.

The addition of an afterbody to the 55° high-drag blunt cone did not appreciably affect its aerodynamic characteristics in the angle-of-attack range of these tests (0° - 15°).

INTRODUCTION

The use of unmanned probes to explore the atmosphere of the planet Mars has been proposed (refs. 1-4). The structure and mean molecular weight of the atmosphere can be determined during entry by on-board measurements of pressure, temperature, and acceleration in appropriate phases of the entry, while the atmospheric composition can be determined by measuring the thermal radiation of the shock layer or by use of a mass spectrometer.

It was originally thought that a ballasted sphere would make an ideal vehicle for this purpose (ref. 1) because of its characteristics of zero lift and constant drag. However, tests (ref. 5) have shown it to be dynamically unsatisfactory, unstable at all Mach numbers from 0.4 to 14.5 and erratic in its angular motions at low speeds. As a substitute for the sphere (intended to retain its basic advantages), a series of sphere-cone models were designed using Newtonian impact theory to have drag independent of angle of attack. From the following relationship from reference 6, $C_{L_\alpha} = C_{p_{max}} - 2C_{D_0}$, a family of spherically blunt cones having constant drag can be derived by setting $C_{L_\alpha} = 0$.

It was the purpose of this investigation to determine the aerodynamic characteristics of three such bodies as well as two higher drag bodies that might be suitable either as probes or landers. The effects of angle of attack on the drag, lift-curve slope, static margin, and the static and dynamic stability were determined for each of the candidate configurations at a Mach number near 10. Some effects of afterbody shape, Mach number, and Reynolds number are noted briefly for one of the high-drag configurations.

These tests were conducted in the Ames Hypervelocity Free-Flight Aerodynamic Facility and the Ames Prototype Hypervelocity Free-Flight Facility.

MODELS

Two classes of model were tested: first, a set of three sphere-cone models designed to have nearly constant drag and a zero lift-curve slope at moderate angles of attack (figs. 1(a), (b), and (c)); and, second, a pair of large-angle blunt cones designed to yield very low m/C_DA (figs. 1(d) and (e)).

The first group was designed using Newtonian impact theory to have constant drag independent of angle of attack and zero lift at angle of attack. The basis for this design is the relationship

$$C_{L_\alpha} = C_{p_{max}} - 2C_{D_0} \qquad \text{(ref. 6)}$$

which, for $C_{p_{max}} = 2$, gives the result that shapes having a drag coefficient of 1 also have a lift-curve slope of 0. The result is a family of cones of varying angle and bluntness starting with a sharp-nosed 45° half-angle cone and ending with a hemisphere, as shown in figure 2.

The first two models were selected on this basis and had cone half-angles (θ_c) of 44.1° and 40.8°, nose-bluntness ratios (r_n/r_b) of 0.33 and 0.67, and center-of-gravity locations (X_{cg}/d) of 0.32 and 0.28 (from the model nose), respectively, as shown in figures 1(a) and (b).

The third zero-lift model was designed to have zero lift at a small finite angle of attack on the premise that since the model would normally be oscillating during reentry, it might be possible to extend the angle-of-attack range in which the lift was essentially zero and the drag variation acceptable. This was accomplished by designing a shape with drag coefficient slightly less than 1($C_D \neq 0$) which from the above equation gave a slightly positive lift-curve slope ($0 < C_{L_\alpha} << 1$) at $\alpha = 0°$. These considerations resulted in a model with a cone half-angle of 27°, a nose bluntness of 0.95, and a center-of-gravity location of 0.27 (fig. 1(c)).

The high-drag configurations (also blunt cones) had cone half-angles of 55° and 60°, nose-bluntness ratios of 1.0 and 0.2, and centers of gravity at 0.17 and 0.23 diameter from the nose, respectively, as shown in figures 1(d) and (e). The 55° cone was also tested with an afterbody consisting of a 30° half-angle spherically blunted cone with a bluntness ratio (r_a/r_b) of 0.5. The center of gravity for this configuration (fig. 1(f)) is located at the point of maximum diameter, 0.24 diameter from the nose. The 60° cone had a corner-radius ratio (r_c/r_b) of 0.1, whereas all other models had sharp corners.

With the exception of model F, these models were homogeneous so that their centers of gravity fell at their respective centers of volume. Model F, however, was bimetallic, as noted in figure 1(f); thus its center of gravity was not coincident with the center of volume.

Photographs of the models and two typical sabots are shown in figure 3. The sabot shown in figure 3(d) is canted 10° to launch the model at an angle of attack.

The model geometries are summarized in table 1.

TESTS

Model configurations A through E were tested in free flight, in still air, in the Ames Hypervelocity Free-Flight Aerodynamic Facility at Mach numbers near 10 and at Reynolds numbers near 300,000, based on the model diameter and free-stream air properties. Tests of configuration F were also made in free flight, in still air, but in the Ames Prototype Hypervelocity Free-Flight Facility at Mach numbers from 3 to 16 and for Reynolds numbers from 160,000 to 590,000.

Table 2 lists the test conditions.

Model Launching

The models tested in the aerodynamic facility were launched from a 25.4 mm (1 in.) diameter deformable-piston, light-gas gun (ref. 7). The models tested in the prototype facility were fired from a similar gun, 12.7 mm

(0.5 in.) in diameter. The models were supported in the guns by means of four-piece polycarbonate plastic (Lexan) sabots (fig. 3).

Instrumentation

Shadowgraphs were obtained in orthogonal planes at 16 observation stations over a ballistic flight of 23 meters (75 ft) (aerodynamic facility) and at 11 observation stations for a ballistic flight of 12 meters (40 ft) (prototype facility). The photographic observation stations in each of the facilities contain accurately calibrated fiducial systems so that the model spatial position and angular orientation are determined accurately over the entire length of the flight. Electronic chronographs measured the time of flight between stations.

DATA REDUCTION

A computer program, described in detail in reference 8, was used to determine the aerodynamic coefficients of each configuration by analyzing their free-flight motions. This data-reduction program uses the time-distance data of each flight to determine drag coefficient and the linear differential equation of motion given by Nicolaides (ref. 9) to determine the lift-curve slope and the static and dynamic stability. This assumption of linear aerodynamics does not prevent the use of this method for bodies with nonlinear stability coefficients. For models having nonlinear coefficients, the above method is used to reduce data from several flights at different amplitudes. These quasilinear coefficients for various angle-of-attack amplitudes are then used in an additional program (also described in ref. 8) to obtain the desired nonlinear coefficients as a function of angle of attack.

Two representative pitching and yawing motions from the present tests, as viewed in the α-β plane, are shown in figure 4. The angles of attack and sideslip determined from shadowgraphs at each station are indicated by the circular symbols. The curves show the theoretical motions which best fit the experimental data; the asterisks are the theoretical points that correspond to the experimental values.

RESULTS AND DISCUSSION

The aerodynamic coefficients C_D, C_m, C_L, ξ, $C_{m_q} + C_{m_{\dot{\alpha}}}$, and the center-of-pressure location determined experimentally are presented in figures 5 through 13 for the zero lift models A, B, and C, and in figures 14 through 22 for the high-drag models D and E. Additional data for one of the high-drag configurations, model F, showing the effect of afterbody shape, Mach number, and Reynolds number are presented in figures 23 through 25.

Zero-Lift Bodies (Sphere Substitutes)

The design requirements for the sphere-substitute bodies (A, B, and C) are drag coefficients ($\approx$1) and lift-curve slopes ($\approx$0) which are essentially invariant with pitching amplitude - at least for moderate pitch amplitudes. The experimental data in figure 5 show that the drag coefficients were essentially constant from $\alpha = 0°$ to 14° for each of the three models, varying only by about 1 percent. These data also show that the drag coefficient decreased with increasing bluntness and decreasing cone angle. It should be noted, however, that this last observation is pertinent only because of the restrictions placed on the variation of cone angle and bluntness due to the specification of zero lift-curve slope. Drag data collected from a number of sources (refs. 10 through 15), and presented in figure 6, show that for either a sharp cone or cones with constant bluntness ratio, a decrease in cone angle is accompanied by a decrease in drag coefficient. These data also show that for cone half-angles below some critical value a change in nose bluntness can have a large effect on the drag coefficient. Thus it becomes apparent, with regard to figure 6, that the decrease in drag coefficient between models A and B is due primarily to the decrease in cone angle and is influenced only slightly by the difference in bluntness. However, the further decrease in drag of model C due to decreasing cone angle is largely offset by the increase in nose bluntness.

The drag data in figure 6 are compared with results of several theoretical calculations (refs. 16-19) with the following results:

1. The drag of pointed cones at zero angle of attack is predicted with good accuracy by conical flow theory (ref. 16) up to the cone angle for which the bow wave becomes detached.

2. In this same cone-angle range, the method of Rakich (ref. 17) can be used to predict the effect of nose bluntness ratio for bluntness ratios from 0 to 1.0. This method shows that for small amounts of bluntness ($r_n/r_b = 0.2$) the effect of bluntness on drag is negligible and that for a given amount of bluntness the effect of bluntness decreases with increasing cone angle.

3. For the range of cone angles where the bow wave is detached for all bluntness ratios the method of integral relations (ref. 18) and the method of Kaattari (ref. 19) do a reasonable job of predicting the drag coefficient. In this cone-angle range the effect of bluntness is negligible.

Although the theory used to design the sphere-substitute shapes specified a drag coefficient of 1.0 and a $C_{p_{max}}$ of 2.0 to obtain a lift-curve slope of 0 (ref. 6) only model A had a drag coefficient of approximately 1.0 (fig. 5). The other two models, having smaller cone angles and larger bluntness ratios, are more nearly approximated if a modified Newtonian pressure coefficient $\left(C_{p_{max}} = 1.8\right)$ is used.

For pitch amplitudes up to 20°, the data presented in figure 7 show that models A and B do in fact have nearly zero lift-curve slopes, as desired.

Model C, however, although having nearly zero lift-curve slope, does show a significant variation of the lift-curve slope with pitching amplitude, becoming increasingly negative with increasing amplitude.

These lift data and the drag data in figure 5 show that, for models A and B, it was possible to design a model with constant drag and nearly zero lift at least for the pitching amplitudes of these tests. The design philosophy used for model C, however, did not result in lift-curve slopes nearer to zero at the higher amplitudes than those obtained for models A and B, as was expected.

Analyzing these lift data by the method presented in reference 20, for nonlinear moments, results in the variation of C_L versus α shown in figure 8. For angles of attack to about 10°, all three configurations had lift coefficients between +0.01 and -0.017. At angles greater than 10°, the lift coefficients for model C decreased quite rapidly with increasing angle of attack.

The static stability $\left(C_{m_\alpha}\right)$ data in figure 9 show a slight decrease in stability with increasing pitch amplitude for models A and B, but for model C the stability remains essentially constant.

Analysis of these nearly linear moment data by the nonlinear method of reference 20 shows, as expected, nearly linear variations of C_m with α (fig. 10). Figures 9 and 10 also show calculated values of C_{m_α} and C_m for model A with the center of gravity moved forward from 32 to 28 percent of the diameter aft of the nose to match the center-of-gravity locations of models B and C. These data show that for pitch amplitudes below 10° the static stability of models A and B were essentially the same.

The lift and moment coefficients (figs. 8 and 10) determined from the experimental data by the method of reference 20, and the drag coefficients (fig. 5) have been used to evaluate static margins $[(X_{cp} - X_{cg})/d]$ for models A, B, and C, which are presented in figure 11. These data (figs. 9 and 11) show that for model A a decrease in static stability with increasing pitch amplitude occurred with no discernible change in the static margin; for model B a decrease in stability was accompanied by a corresponding decrease in the static margin; and for model C the stability remained constant with an increase in the static margin.

Also shown in figure 11 are static margins predicted for the models by Newtonian impact theory. These theoretical predictions agree well with the calculated data for all three models but do not predict the change in the center-of-pressure location as a function of the changing amplitude for models B and C.

The dynamic damping parameter, ξ, and the dynamic stability, $C_{m_q} + C_{m_{\dot{\alpha}}}$, for the three zero lift models (A, B, and C) are presented in figures 12 and 13, respectively. These data show that models A and B were both dynamically

stable and that the stability was nearly constant for the pitching amplitudes of these tests. Model C, however, appears definitely to be dynamically unstable (ξ positive).

High-Drag Bodies

The experimentally determined drag coefficients in figure 14 for models D and E (the two high-drag models) show that model E with 60° cone half-angle had about a 4-percent higher drag coefficient than did model D (55°). It can be seen from figure 6 that both configurations lie in or near the regime where the bow shock is detached for sharp cones and the bluntness ratio has a negligible effect on the drag. The drag coefficient obtained for model E, although predicted well by Newtonian theory $\left(C_{p_{max}} = 2.0, \text{ fig. } 14\right)$, is somewhat lower than that shown in figure 6 for a comparable model without the shoulder radius. This reduction in drag is apparently due to a change in the flow field in the vicinity of the rounded shoulders.

The lift-curve slopes $\left(C_{L_\alpha}\right)$ and the lift curves derived from them by the nonlinear method of reference 20 are presented in figures 15 and 16. There appears to be no significant difference between the two configurations with respect to lift, except for values of C_L at angles of attack above about 12°. It should be pointed out, however, that in the angle range in which these lift curves diverge, C_L is not defined as well as at lower angles because the nonlinear terms used in the analysis become dominant. These terms may be spurious, since the lift-curve slopes measured were nearly constant over the amplitude range of these tests (to $\alpha = 15.5°$) at approximately -1.0.

Static-stability data $\left(C_{m_\alpha}\right)$ for models D and E (fig. 17) show that both models were statically stable for all of the pitching amplitudes of these tests. However, these data also show that for the 55° blunt cone (model D), the stability decreased with increasing pitch amplitude and for the 60° blunt cone (model E), the stability increased. Of the five models tested, only model E became more stable with increasing pitch amplitude. Since model E was the only one of the five models to have a rounded shoulder, the pressure distribution in the vicinity of the shoulder could be influenced by a movement of the separation point, whereas for the sharp cornered models the separation is fixed at the corner.

Pitching-moment coefficients calculated from the experimental data by the method of reference 20, based on a linear plus a cubic representation, are presented in figure 18.

These moment data (fig. 18) and the drag and lift coefficients in figures 14 and 16 were used to calculate center-of-pressure locations (X_{cp}/d) and static margins $[(X_{cp} - X_{cg})/d]$ for models D and E. The data (figs. 19 and 20, respectively) show the rate of change of the center of pressure with respect to angle of attack to be nearly the same for each model even though the rate of change of the pitching-moment-curve slopes with angle of attack is

considerably different (see fig. 17). These data also show that the center-of-pressure location for the 55° cone is approximately 40 percent of the diameter farther aft than that for the 60° cone. The centers of pressure of the two models predicted by Newtonian impact theory do not show this large difference. In fact, Newtonian theory predicts no difference at all.

It can be seen in figures 14, 17, 19, and 20 that Newtonian theory does a reasonable job of predicting the aerodynamic characteristics of the 60° blunt cone but does a poor job of predicting the characteristics for the 55° blunt cone. The reason may be that for the 60° cone the bluntness is small ($r_n/r_b = 0.20$), the bow shock wave is essentially conical and the shock-wave stand-off distance is small; whereas, for the 55° cone the bluntness is large ($r_n/r_b = 1.00$), the bow shock wave is essentially spherical, and the stand-off distance from the body is significant. It is apparently this large effect of bluntness that moved the center of pressure so much farther aft for the 55° cone than for the 60° cone. The extreme case of a right circular cylinder illustrates this well, because Newtonian theory predicts no stability, yet this shape is highly stable.

The damping parameter (ξ) and the dynamic stability $\left(C_{m_q} + C_{m_{\dot{\alpha}}}\right)$ for models D and E as a function of pitching amplitude are presented in figures 21 and 22, respectively. Both models are dynamically stable with nearly equal damping characteristics which are essentially independent of pitching amplitude for the amplitudes of these tests. It should be noted that a damping parameter of -4 represents a convergence in the model motion of approximately 3 to 4 percent per cycle.

The aerodynamic coefficients determined for model D are compared in figures 23 to 25 with coefficients for an identical forebody with a 30° half-angle blunt cone afterbody (model F) and a center-of-gravity location 7-1/2° farther aft.

The drag coefficients (fig. 23) are nearly the same. However, the drag of model D decreases a little more rapidly with increasing angle of attack.

The two models have identical static stability (fig. 24) when compared for identical moment centers (C_{m_α} for model D, fig. 19, was transferred to match the moment center of model F for these comparisons). It should be pointed out at this time that the fiducial system in the facility in which the tests of model F were performed (Ames Prototype Hypervelocity Free-Flight Facility) is not sufficiently detailed to enable the accurate measurement of the model translation in the y and z directions required for determining the lift-curve slope. However, since the drag coefficients for model F (with afterbody) did not decrease with increasing angle of attack as much as that for model D and since the static stability $\left(C_{m_\alpha}\right)$ was the same for both models, it can be reasoned that the presence of the afterbody did not affect the normal force but did slightly increase the axial force at the higher angles of attack.

The damping parameter, ξ, for these two models (fig. 25) is the same, within measurement accuracy, despite the moment-center differences. Unpublished data for model F in the transonic region have shown that a 5-percent forward shift in the center-of-gravity location resulted in a significant increase in the dynamic stability. Similar improvement at a Mach number of 10 is not apparent from the data presented herein.

Figures 23 to 25 also include data for model F at Mach numbers of 3 and 16 and for Reynolds numbers from 200,000 to 400,000. The only significant effect of these variations in Mach number and Reynolds number was in the static stability for a Mach number of 3. At this Mach number there was a considerable decrease in static stability (-0.145) with respect to that at a Mach number of 10 (-0.25). These Mach number 3 results compare favorably with unpublished data obtained at a Mach number of 1.2.

CONCLUSIONS

The static and dynamic aerodynamic characteristics of three zero lift-curve slope, constant-drag bodies and two higher drag bodies having possible application as Mars probe-lander configurations have been determined experimentally in free flight, in still air. The test data indicate the following:

1. Using the Newtonian relationship $C_{L_\alpha} = C_{P_{max}} - 2C_{D_0}$ it is possible to design a family of spherically blunt cones that have essentially constant drag and nearly zero lift at angles of attack less than 15°. The three configurations designed on the basis of the above relationship show, experimentally, that the combination of decreasing cone angle and increasing nose bluntness required by these constraints resulted in a decrease in the dynamic stability. In fact, for the three models tested the dynamic stability varied from stable to unstable.

2. Of the two high-drag models tested (55° and 60° blunt cones), the 60° cone had the higher drag by about 4 percent but the 55° cone was the more stable. Of the five configurations investigated, only the 60° cone showed increasing static stability with increasing angle of attack. The lift-curve slope and dynamic stability were nearly the same for both the 55° and 60° shapes, and in both cases the models were statically and dynamically stable.

3. The addition of an afterbody to the 55° cone did not appreciably affect the aerodynamics for the range of angles of attack of these tests.

4. For all models, the static and dynamic aerodynamic characteristics were orderly and generally nearly linear and displayed no unusual characteristics.

Ames Research Center
National Aeronautics and Space Administration
Moffett Field, California 94035, Sept. 19, 1969

REFERENCES

1. Seiff, Alvin; and Reese, David E., Jr.: Defining Mars' Atmosphere - A Goal for Early Missions. Astronaut. Aeron., Feb. 1965.

2. Peterson, Victor L.: A Technique for Determining Planetary Atmosphere Structure From Measured Accelerations of an Entry Vehicle. NASA TN D-2669, 1965.

3. Roberts, Leonard: Entry Into Planetary Atmospheres. Astronaut. Aeron., vol. 2, Oct. 1964, pp. 22-29.

4. Sommer, Simon C.; Boissevain, Alfred G.; Yee, Layton; and Hedlund, Roger C.: The Structure of an Atmosphere From On-Board Measurements of Pressure, Temperature, and Acceleration. NASA TN D-3933, 1967.

5. Short Barbara J.: Dynamic Flight Behavior of a Ballasted Sphere at Mach Numbers From 0.4 to 14.5. NASA TN D-4198, 1967.

6. Chapman, Gary T.: A Simple Relationship Between the Drag Near Zero Lift and the Initial Normal-Force-Curve Slope Obtained From Newtonian Theory. AIAA J., vol. 3, no. 6, June 1965, pp. 1194-1195.

7. Curtis, John S.: An Accelerated Reservoir Light-Gas Gun. NASA TN D-1144, 1962.

8. Malcolm, Gerald N.; and Chapman, Gary T.: A Computer Program for Systematically Analyzing Free-Flight Data to Determine the Aerodynamics of Axisymmetric Bodies. NASA TN D-4766, 1968.

9. Nicolaides, John D.: On the Free-Flight Motion of Missiles Having Slight Configurational Asymmetries. BRL Rep. 858, June 1953.

10. Chapman, Gary T.; and Jackson, Charles T., Jr.: Measurement of the Heat Transfer to Bodies of Revolution in Free-Flight by Use of a Catcher Calorimeter. NASA TN D-1890, 1963.

11. Penland, Jim A.: A Study of the Stability and Location of the Center of Pressure on Sharp, Right Circular Cones at Hypersonic Speeds. NASA TN D-2283, 1964.

12. Nichols, James O.; and Nierengarter, Edward A.: Aerodynamic Characteristics of Blunt Bodies. JPL TR No. 32-677, 1964.

13. Intrieri, Peter F.: Study of the Stability and Drag at Mach Numbers From 4.5 to 13.5 of a Conical Venus-Entry Body. NASA TN D-2827, 1965.

14. Chapman, Gary T.; Terry, James E.; and Bruin, Scott: Experimental Aerodynamic Characteristics of 10 Short Axisymmetric Bodies at Mach Numbers of 5 to 15. NASA TN D-2848, 1965.

15. Intrieri, Peter F.: Experimental Stability and Drag of a Pointed and a Blunted 30° Half-Angle Cone at Mach Numbers From 11.5 to 34 in Air. NASA TN D-3193, 1966.

16. Staff of Computing Section (under the direction of Zdenek Kopal): Table of Supersonic Flow Around Yawing Cones. Tech. Rep. 3, Center of Analysis, M. I. T., Cambridge, 1947.

17. Rakich, John V.: Numerical Calculation of Supersonic Flows of a Perfect Gas Over Bodies of Revolution at Small Angles of Yaw. NASA TN D-2390, 1964.

18. Inouye, Mamoru; and Marvin, Joseph G.: Comparison of Experimental and Theoretical Shock Shapes and Pressure Distributions on Flat-Faced Cylinders at Mach 10.5. NASA TN D-4397, 1968.

19. Kaattari, George E.: Predicted Gas Properties in the Shock Layer Ahead of Capsule-Type Vehicles at Angles of Attack. NASA TN D-1423, 1962.

20. Ramussen, Maurice L.; and Kirk, Donn B.: On the Pitching and Yawing Motion of a Spinning Symmetric Missile Governed by an Arbitrary Non-linear Restoring Moment. NASA TN D-2135, 1964.

TABLE 1.- SUMMARY OF MODEL GEOMETRIES

Model class	Constant drag (zero lift)			High drag		
Configuration	A	B	C	D	E	F
Cone half-angle (θ_c), deg	44.1	40.8	27.0	55.0	60.0	55.0
Bluntness ratio (r_n/r_b)	0.33	0.67	0.95	1.00	0.20	1.00
Corner radius ratio (r_c/r_b)	0	0	0	0	0.10	0
Center of gravity from nose $\left(X_{cg}/d\right)$	0.32	0.28	0.27	0.17	0.23	0.24
Afterbody cone half-angle (θ_a), deg	90	90	90	90	90	30
Afterbody bluntness ratio (r_a/r_b)	∞	∞	∞	∞	∞	0.25
Nominal diameter, cm	2.032	2.032	2.032	2.032	2.032	1.016

TABLE 2.- MODEL MEASUREMENTS, TEST CONDITIONS, AND RESULTS

(a) Aerodynamic facility

Run	C_D	$-C_{m_\alpha}$, per rad	C_{L_α}, per rad	ξ	$C_{m_q}+C_{m_{\dot\alpha}}$	M_∞	$Re\times10^{-6}$	$\rho_\infty\times10^3$, g/cm^3	α_{rms}, deg	α_m, deg	α_m/α_{min}	α,β dev., deg	y,z dev., cm	d, cm	$m\times10^{-1}$, g	$I_y\times10^{-1}$, g-cm^2	I_y/I_x	md^2/I_y	$\rho_\infty A/2m\times10^4$, cm^{-1}
Model A; θ_c = 44.1°																			
88	0.984	0.275	-0.112	-0.817	-0.092	10.86	0.3211	0.0768	5.31	7.66	23.2	0.27	0.0117	2.0368	0.9340	0.1872	0.6360	20.70	0.1340
98	.989	.275	-.831	-6.071	-.379	10.00	.3210	.0761	1.89	2.67	11.6	.22	.0117	2.0356	.9200	.1829	.6368	20.84	.1346
104	.991	.275	-.118	-2.728	-.184	10.88	.3181	.0762	6.24	8.92	14.9	.36	.0099	2.0366	.9213	.1832	.6353	20.86	.1346
111	.985	.276	-.005	-2.396	-.161	10.66	.3111	.0761	8.70	11.96	4.3	.29	.0076	2.0325	.8999	.1768	.6365	21.02	.1373
112	.970	.265	-.071	-2.355	-.164	10.75	.3169	.0767	8.47	10.75	2.3	.35	.0089	2.0356	.9275	.1859	.6377	20.67	.1345
113	.987	.270	-.191	-1.103	-.110	10.82	.3176	.0764	8.60	12.44	37.7	.23	.0129	2.0366	.9171	.1831	.6367	20.77	.1356
114	.976	.267	-.041	-7.589	-.417	10.64	.3112	.0763	8.38	11.50	41.1	.23	.0099	2.0325	.9224	.1845	.6378	20.66	.1342
139	.970	.259	-.082	.241	-.039	10.78	.3154	.0763	13.79	18.86	4.8	.37	.0127	2.0335	.9241	.1847	.6364	20.69	.1341
140	.986	.266	-.031	-3.035	-.196	10.92	.3207	.0765	12.46	17.04	33.40	.34	.0135	2.0330	.9195	.1834	.6376	20.72	.1351
141	.986	.273	.051	-2.235	-.153	10.72	.3155	.0766	11.98	15.77	2.6	.29	.0147	2.0345	.9209	.1840	.6368	20.72	.1352
142	.966	.265	-.195	-2.710	-.186	10.74	.3152	.0764	13.30	18.10	5.6	.29	.0122	2.0356	.9222	.1839	.6373	20.78	.1347
Model B; θ_c = 40.8°																			
89	.901	.315	-.226	-2.247	-.166	10.94	.3260	.0776	3.24	4.56	18.2	.41	.0099	2.0351	.9948	.2030	.6294	20.30	.1268
100	.902	.308	.239	-1.622	-.113	11.06	.3286	.0774	4.39	6.20	77.5	.46	.0132	2.0340	.9941	.2026	.6275	20.30	.1265
105	.904	.308	.087	-3.827	-.229	11.05	.3260	.0771	5.77	8.07	25.3	.46	.0122	2.0292	.9848	.1996	.6307	20.32	.1267
115	.909	.298	.035	-1.035	-.094	10.77	.3187	.0772	8.67	11.44	3.2	.33	.0114	2.0333	.9918	.2022	.6290	20.28	.1263
116	.908	.299	.115	-3.847	-.229	10.47	.3104	.0772	8.71	10.97	1.97	.33	.0107	2.0351	.9986	.2040	.6283	20.27	.1258
123	.907	.298	-.027	-5.914	-.336	10.78	.3182	.0770	9.44	12.65	4.2	.45	.0152	2.0330	.9882	.2003	.6293	20.39	.1265
124	.909	.303	.159	-.576	-.065	10.71	.3167	.0771	8.30	11.31	6.3	.30	.0127	2.0343	.9936	.2025	.6277	20.30	.1261
143	.914	.286	.205	.639	-.003	10.73	.3176	.0773	12.75	16.41	2.3	.30	.0079	2.0290	.9890	.2006	.6275	20.30	.1264
144	.918	.284	.098	.811	-.001	10.60	.3139	.0773	11.77	16.50	7.1	.41	.0099	2.0302	.9826	.1988	.6291	20.37	.1274
145	.915	.292	.127	-4.681	-.267	10.94	.3228	.0773	12.19	15.67	2.3	.34	.0137	2.0239	.9675	.1932	.6259	20.51	.1285
146	.919	.290	-.008	.989	.003	10.81	.3209	.0774	12.45	16.89	4.3	.27	.0165	2.0320	.9929	.2020	.6287	20.29	.1264
Model C; θ_c = 27°																			
87	.858	.199	-.027	7.258	.350	11.20	.3317	.0772	3.62	5.01	12.5	.32	.0081	2.0335	1.234	.2801	.6240	18.22	.1016
102	.858	.197	-.069	6.932	.328	11.06	.3270	.0769	7.78	10.88	121.1	.47	.0107	2.0371	1.234	.2801	.6242	18.29	.1015
103	.855	.205	.058	-5.679	-.355	11.13	.3273	.0767	4.70	6.46	29.4	.31	.0094	2.0348	1.232	.2795	.6148	18.26	.1012
106	.867	.203	-.005	5.027	.228	11.05	.3247	.0768	8.05	11.16	23.7	.49	.0089	2.0295	1.223	.2765	.6234	18.22	.1015
125	.866	.196	-.231	-1.337	-.134	11.12	.3266	.0767	10.21	12.49	1.7	.37	.0101	2.0310	1.222	.2764	.6245	18.24	.1017
129	.859	.202	-.192	5.023	.217	11.15	.3248	.0762	8.05	11.36	4.8	.36	.0140	2.0315	1.222	.2758	.6214	18.28	.1011
130	.863	.201	-.127	.488	-.028	10.82	.3179	.0767	8.21	10.87	2.4	.39	.0097	2.0325	1.229	.2785	.6234	18.23	.1012
147	.859	.199	-.247	5.023	.215	11.20	.3314	.0772	13.21	18.86	15.6	.42	.0195	2.0320	1.233	.2793	.6240	18.23	.1014
148	.861	.197	-.360	4.431	.176	11.18	.3309	.0772	13.45	18.10	2.7	.44	.0193	2.0302	1.221	.2757	.6223	18.25	.1024
149	.869	.199	-.388	1.650	.022	11.20	.3297	.0771	12.52	17.82	21.2	.32	.0157	2.0251	1.228	.2775	.6238	18.15	.1011
150	.865	.199	-.211	6.888	.318	11.04	.3266	.0772	13.94	18.31	2.5	.37	.0157	2.0290	1.222	.2755	.6234	18.26	.1022
Model D; θ_c = 55°																			
86	1.330	.278	-1.068	-.065	-.104	10.09	.3023	.0783	4.44	6.24	16.9	.40	.0101	2.0300	.5817	.1007	.5449	23.81	.2177
92	1.362	.285	-1.275	2.249	-.016	10.39	.3122	.0786	2.53	3.30	19.6	.27	.0109	2.0257	.5745	.0981	.5411	24.03	.2206
94	1.360	.275	-.972	.688	-.068	10.12	.3067	.0790	1.57	2.22	12.3	.44	.0104	2.0345	.5777	.0996	.5432	24.02	.2221
132	1.309	.265	-.894	-3.366	-.233	10.05	.3050	.0791	8.72	12.24	9.6	.36	.0112	2.0323	.5828	.1008	.5429	23.87	.2201
133	1.318	.272	-1.004	-.337	-.112	10.15	.3077	.0790	7.73	10.64	4.3	.34	.0134	2.0330	.5830	.1011	.5427	23.84	.2200
134	1.313	.274	-.964	-3.678	-.249	10.32	.3118	.0790	8.45	11.28	2.9	.29	.0099	2.0277	.5793	.0997	.5436	23.90	.2200
151	1.280	.260	-1.053	-3.942	-.262	10.19	.3058	.0784	11.07	15.27	4.7	.36	.0157	2.0300	.5797	.0998	.5427	23.93	.2189
152	1.288	.263	-1.000	-3.171	-.229	10.25	.3083	.0786	10.49	14.88	213.0	.54	.0124	2.0315	.5828	.1011	.5442	23.80	.2185
153	1.285	.261	-.972	-1.857	-.171	10.31	.3094	.0782	10.90	15.25	8.1	.51	.0127	2.0376	.5812	.1005	.5436	24.01	.2194

TABLE 2.- MODEL MEASUREMENTS, TEST CONDITIONS, AND RESULTS - Concluded

Run	C_D	$-C_{m_\alpha}$, per rad	C_{L_α}, per rad	ξ	$C_{m_q}+C_{m_{\dot\alpha}}$	M_∞	$Re\times10^{-6}$	$\rho_\infty\times10^3$, g/cm^3	α_{rms}, deg	α_m, deg	α_m/α_{min}	α,β dev., deg	y,z dev., cm	d, cm	$m\times10^{-1}$, g	$I_y\times10^{-1}$, g-cm^2,	I_y/I_x	md^2/I_y	$\rho_\infty A/2m\times10^4$ cm^{-1}
Model E; θ_c = 60°																			
90	1.404	0.159	-1.178	-0.977	-0.165	10.17	0.3151	0.0806	3.83	5.37	5.06	0.27	0.0127	2.0340	0.6748	0.1294	0.5440	21.58	0.1940
95	1.436	---	---	-2.027	---	10.39	.3193	.0801	2.30	3.26	54.4	.29	.0137	2.0343	.6720	.1289	.5447	21.57	.1938
96	1.392	.162	-1.098	-2.363	-.226	10.36	.3196	.0804	6.25	8.99	18.7	.50	.0119	2.0338	.6727	.1294	.5453	21.51	.1940
97	1.416	---	---	-5.881	---	9.22	.2828	.0800	2.96	4.24	18.4	.26	.0140	2.0348	.6730	.1291	.5434	21.58	.1932
107	1.357	.167	-1.047	-2.766	-.242	10.41	.3222	.0806	7.55	9.85	2.6	.38	.0091	2.0340	.6728	.1303	.5436	21.36	.1946
108	1.390	.156	-.965	-3.789	-.283	10.17	.3124	.0802	7.07	9.56	4.8	.36	.0096	2.0320	.6599	.1254	.5427	21.73	.1971
109	1.380	.163	-1.059	-3.543	-.277	10.34	.3172	.0801	7.33	9.68	3.1	.27	.0099	2.0328	.6627	.1266	.5452	21.63	.1960
110	1.366	.157	-.951	-2.477	-.221	10.27	.3170	.0803	7.66	8.99	1.5	.29	.0127	2.0363	.6681	.1277	.5429	21.70	.1958
135	1.322	.169	-.881	-3.434	-.262	10.24	.3162	.0804	11.64	15.15	2.6	.31	.0112	2.0338	.6714	.1292	.5438	21.49	.1946
136	1.330	.170	-.914	-1.817	-.188	10.18	.3151	.0806	11.29	15.52	29.9	.24	.0125	2.0356	.6721	.1290	.5433	21.58	.1951
137	1.312	.172	-.897	-4.088	-.291	10.33	.3189	.0804	11.80	15.24	2.6	.35	.0150	2.0356	.6716	.1286	.5435	21.64	.1947
138	1.330	.167	-.919	-3.426	-.264	10.21	.3162	.0807	10.92	14.95	7.6	.26	.0091	2.0348	.6742	.1299	.5443	21.48	.1946
(b) Prototype hypervelocity free-flight facility																			
Model F; θ_c = 55°																			
1525	1.373	.144	---	4.748	---	3.09	.0591	.0998	4.11	6.08	608.0	.20	---	1.0140	.2208	.0144	.8115	15.75	.1824
1526	1.350	.144	---	2.171	---	3.13	.0597	.0995	5.45	7.79	65.0	.18	---	1.0145	.2137	.0137	.8058	16.05	.1882
1522	1.351	.258	---	54.252	---	10.88	.2057	.0989	1.38	2.00	16.7	.25	---	1.0152	.2242	.0145	.7974	15.98	.1786
1523	1.331	.283	---	48.703	---	10.73	.2033	.0990	1.19	1.61	40.2	.41	---	1.0155	.2240	.0144	.7883	16.03	.1790
1530	1.266	.222	---	.543	---	10.16	.1943	.0998	12.51	17.55	8.1	.23	---	1.0155	.2227	.0144	.7912	15.95	.1813
1531	1.250	.222	---	2.217	---	10.55	.2002	.0992	14.53	20.03	5.7	.27	---	1.0155	.2226	.0144	.8026	15.96	.1805
1570	1.324	.237	---	.695	---	10.25	.1997	.1011	8.56	11.91	39.7	.17	---	1.0185	.2265	.0148	.7792	15.92	.1818
1571	1.343	.253	---	-2.782	---	11.00	.2126	.1006	8.17	10.82	3.2	.25	---	1.0160	.2265	.0147	.7871	15.91	.1801
1572	1.362	.258	---	3.008	---	11.21	.2172	.1008	8.97	12.96	9.7	.15	---	1.0157	.2237	.0143	.7775	16.09	.1826
1573	1.330	.245	---	-.091	---	11.17	.2153	.1003	9.41	12.43	2.6	.28	---	1.0160	.2283	.0147	.7747	16.03	.1781
1574	1.358	.258	---	-7.624	---	11.32	.2198	.1009	1.69	2.18	5.5	.37	---	1.0155	.2250	.0144	.7716	16.12	.1816
1595	1.360	.252	---	7.771	---	10.85	.2082	.1001	2.68	3.66	8.9	.33	---	1.0150	.2235	.0142	.7745	16.16	.1812
1596	1.356	.250	---	-11.222	---	10.94	.2130	.1013	2.36	3.22	12.8	.24	---	1.0147	.2253	.0144	.7813	16.06	.1818
1597	1.337	.242	---	10.268	---	11.08	.2136	.1005	5.90	8.14	11.2	.18	---	1.0147	.2240	.0143	.7799	16.08	.1815
1601	1.365	.254	---	8.967	---	10.56	.2031	.1002	3.62	4.98	6.8	.36	---	1.0155	.2277	.0146	.7764	16.06	.1782
1674	1.347	.253	---	-12.817	---	11.05	.2093	.0991	8.58	11.46	3.1	.40	---	1.0152	.2239	.0143	.7986	16.14	.1790
1675	1.327	.252	---	-4.597	---	11.00	.2097	.0997	10.62	14.53	29.1	.36	---	1.0132	.2233	.0142	.7962	16.17	.1799
1676	1.367	.252	---	-.417	---	11.47	.2230	.1014	7.72	9.33	2.7	.29	---	1.0114	.2239	.0146	.8102	15.73	.1819
1677	1.345	.256	---	.491	---	11.62	.2218	.1002	9.49	12.91	1.0	.40	---	1.0084	.2230	.0146	.8180	15.57	.1795
1678	1.347	.242	---	-1.158	---	11.40	.2157	.0992	8.84	11.48	3.2	.24	---	1.0124	.2245	.0142	.7877	16.25	.1778
1679	1.352	.241	---	-3.210	---	11.30	.2191	.1010	8.47	11.44	7.4	.16	---	1.0130	.2215	.0140	.7866	16.21	.1838
1532	1.239	.220	---	.528	---	10.69	.3865	.1885	15.68	22.55	8.0	.51	---	1.0142	.2230	.0143	.7893	16.02	.3414
1533	1.257	.221	---	-.955	---	10.66	.3782	.1861	14.24	20.54	24.2	.57	---	1.0117	.2189	.0142	.8116	15.77	.3417
1534	1.237	.217	---	-1.159	---	10.76	.3810	.1850	16.12	23.27	136.9	.29	---	1.0173	.2256	.0146	.7898	16.03	.3333
1576	1.387	.246	---	-29.117	---	16.07	.3131	.1014	3.59	4.85	5.5	.46	---	1.0147	.2249	.0145	.7814	15.99	.1823
1577	1.372	.284	---	-16.907	---	15.48	.2984	.1005	3.17	3.95	4.1	.58	---	1.0145	.2248	.0144	.7833	16.05	.1807
1578	1.427	.318	---	-8.263	---	16.00	.3133	.1017	.70	.91	4.3	.32	---	1.0160	.2244	.0143	.7891	16.18	.1837

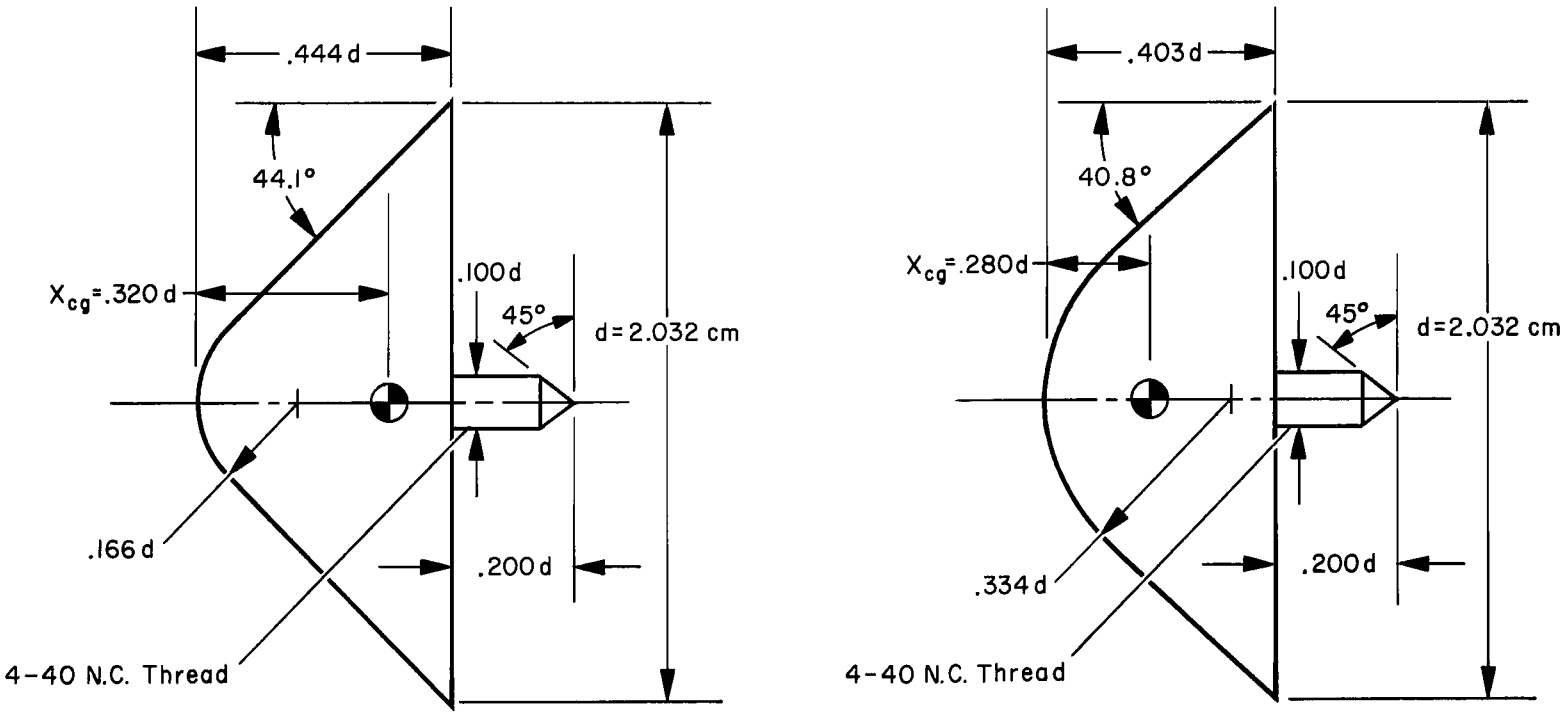

(a) Model A ($X_{cg}/d = 0.32$).

(b) Model B ($X_{cg}/d = 0.28$).

Figure 1.- Model configurations.

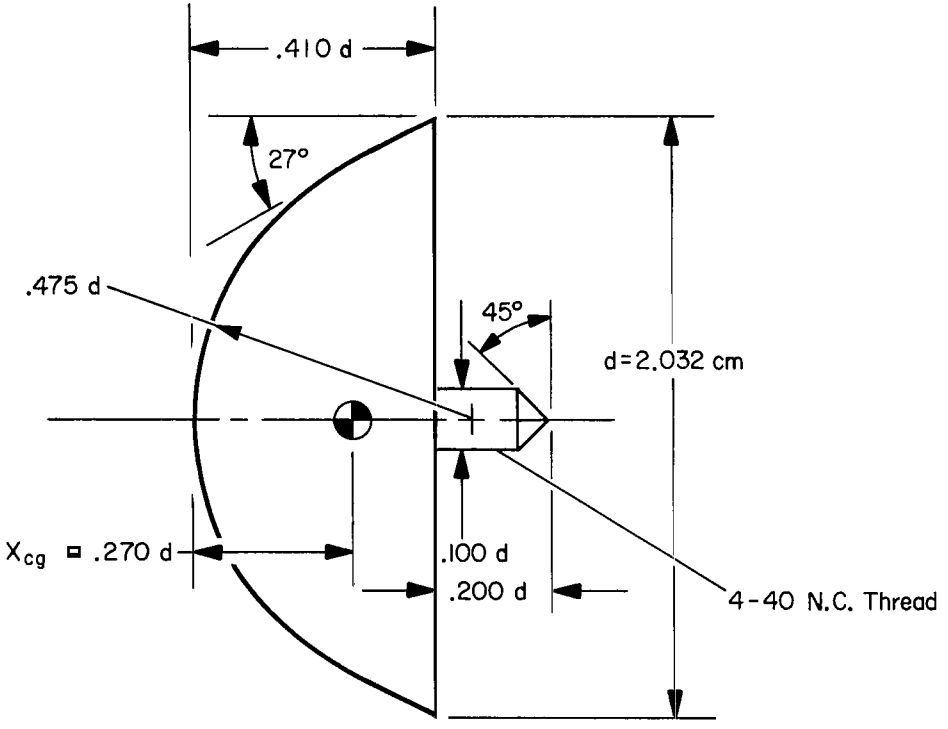

(c) Model C ($X_{cg}/d = 0.27$).

Figure 1.- Continued.

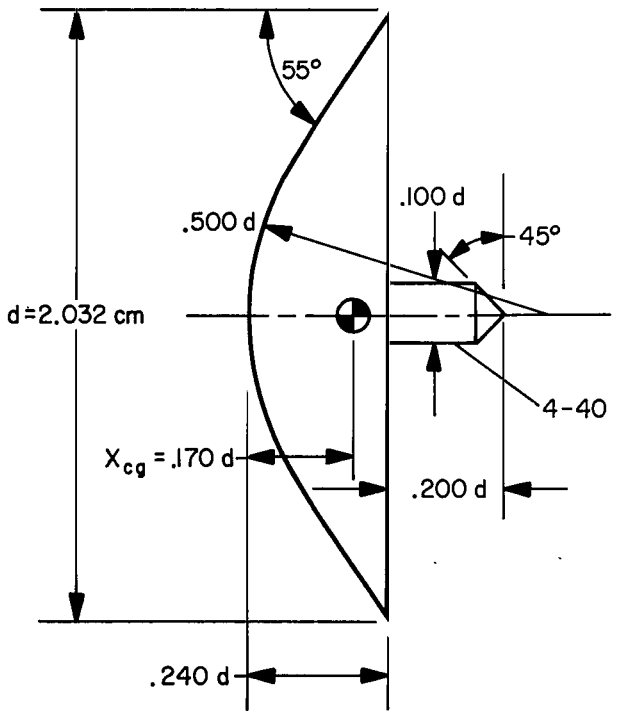

(d) Model D ($X_{cg}/d = 0.17$).

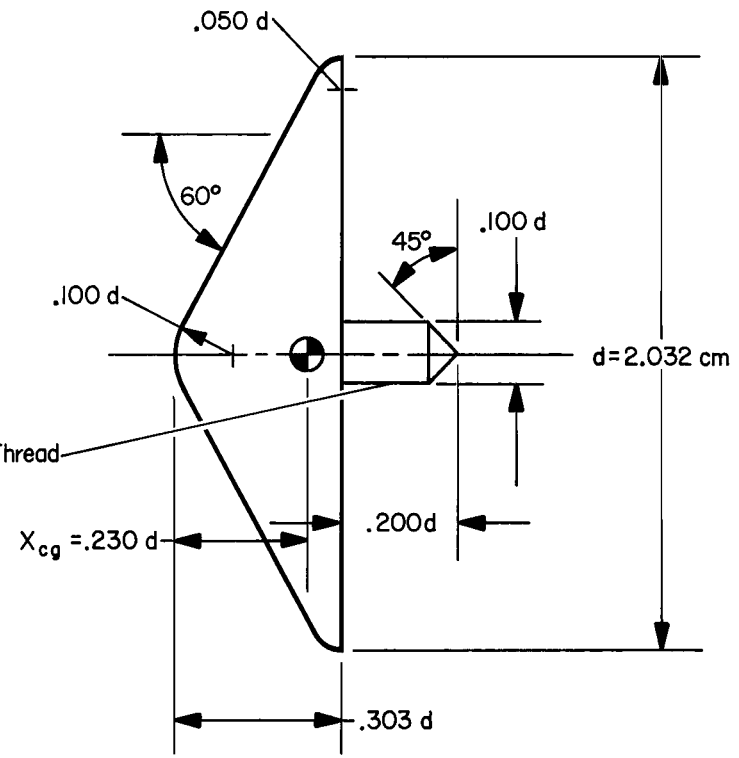

(e) Model E ($X_{cg}/d = 0.23$).

Figure 1.- Continued.

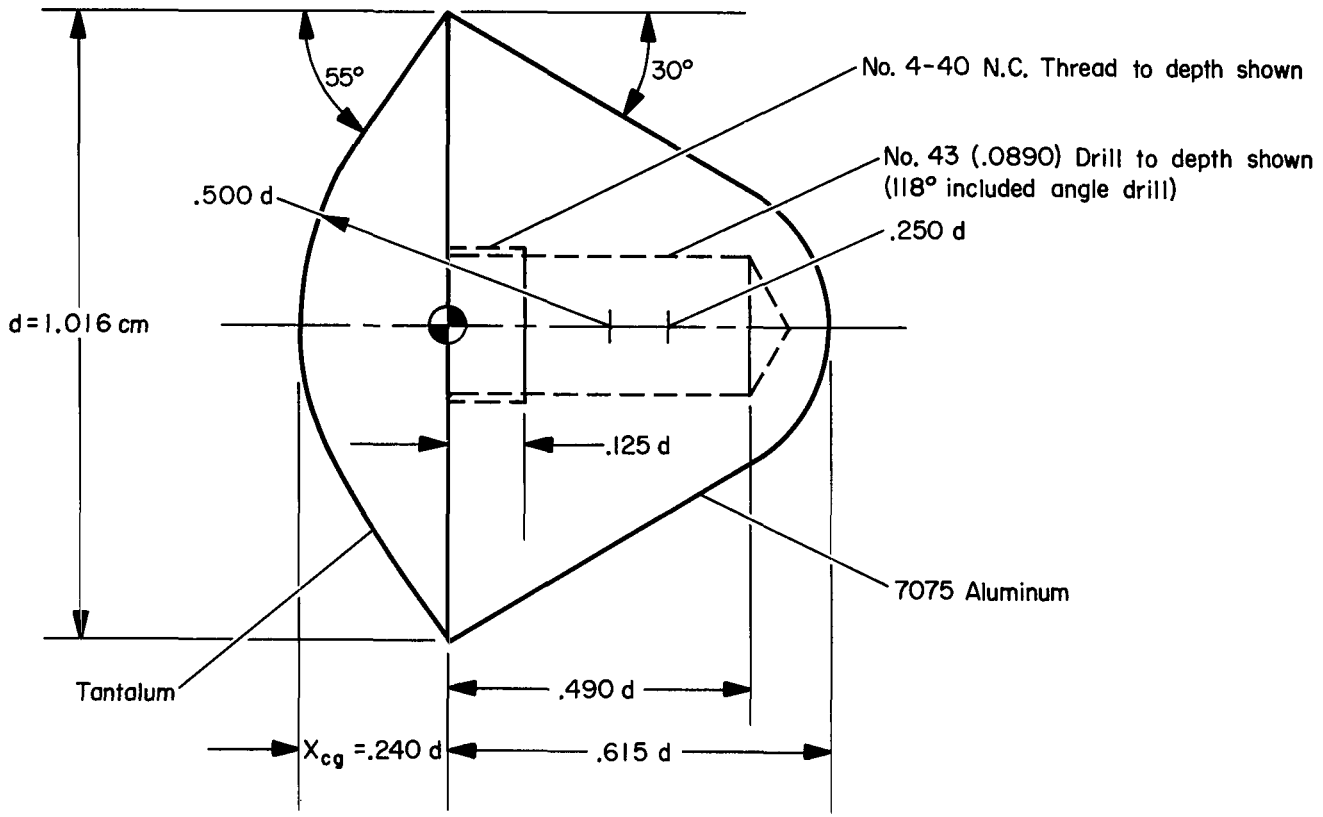

(f) Model F ($X_{cg}/d = 0.24$).

Figure 1.- Concluded.

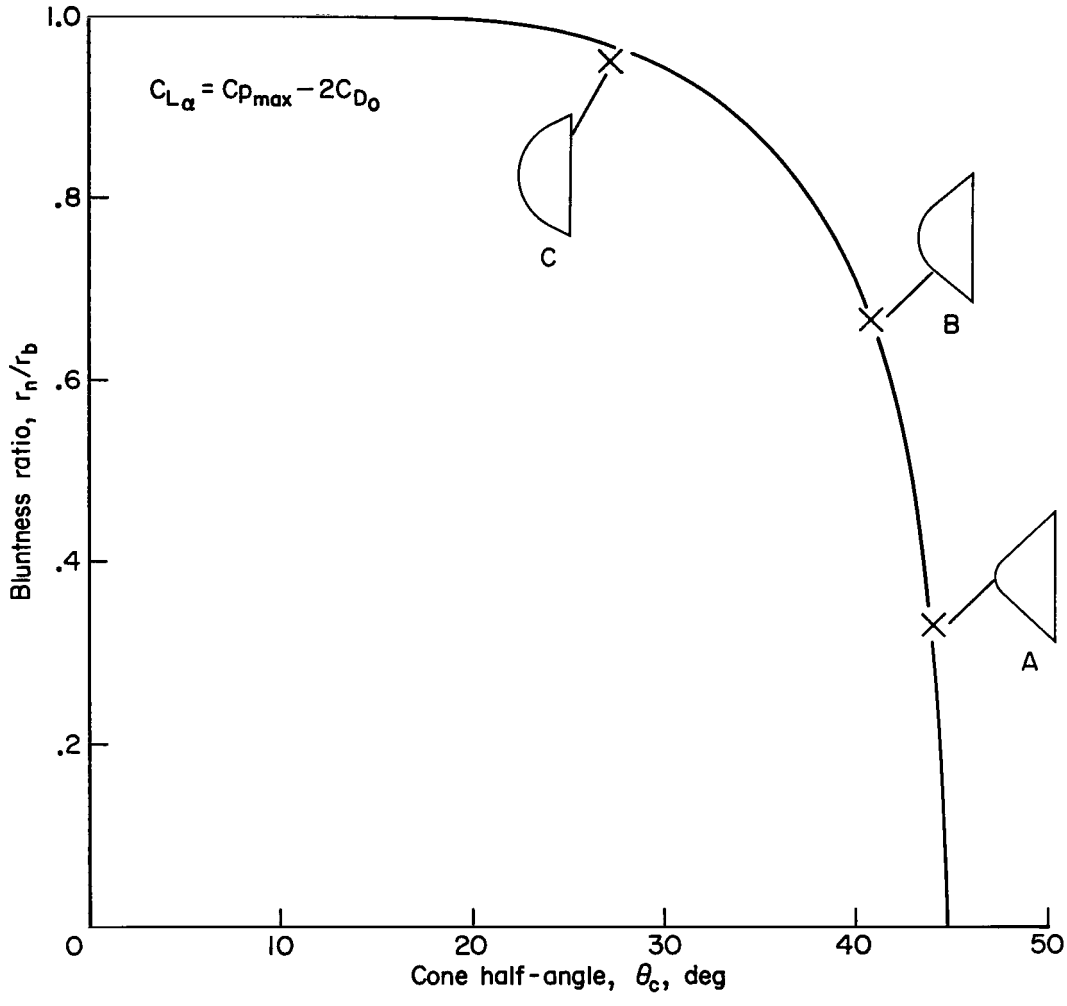

Figure 2.- The relationship between nose bluntness and cone half-angle for models having $C_D = 1.0$ and $C_{L_\alpha} = 0$.

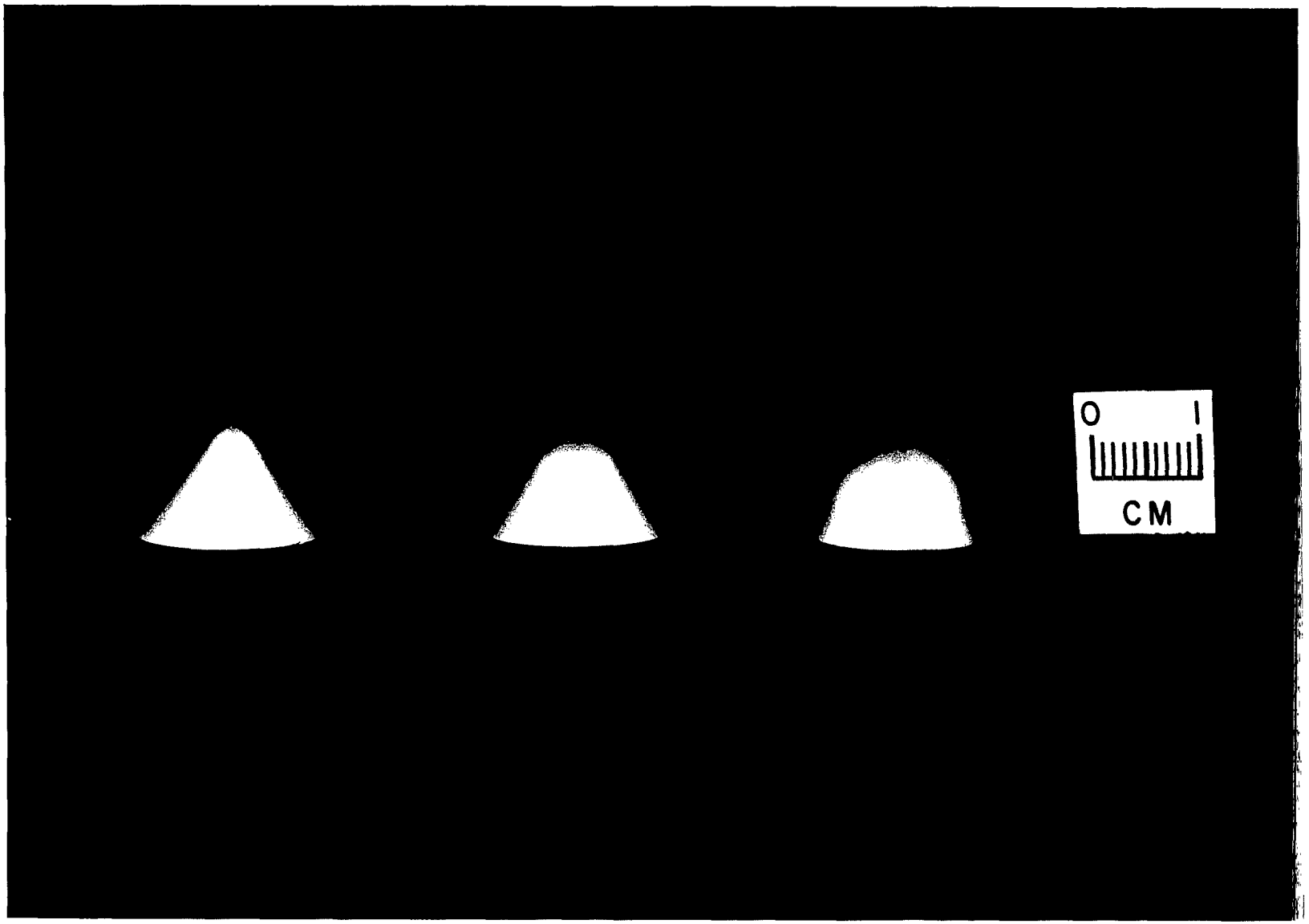

A-36135

(a) Zero lift constant drag bodies.

Figure 3.- Photographs of models and typical sabots.

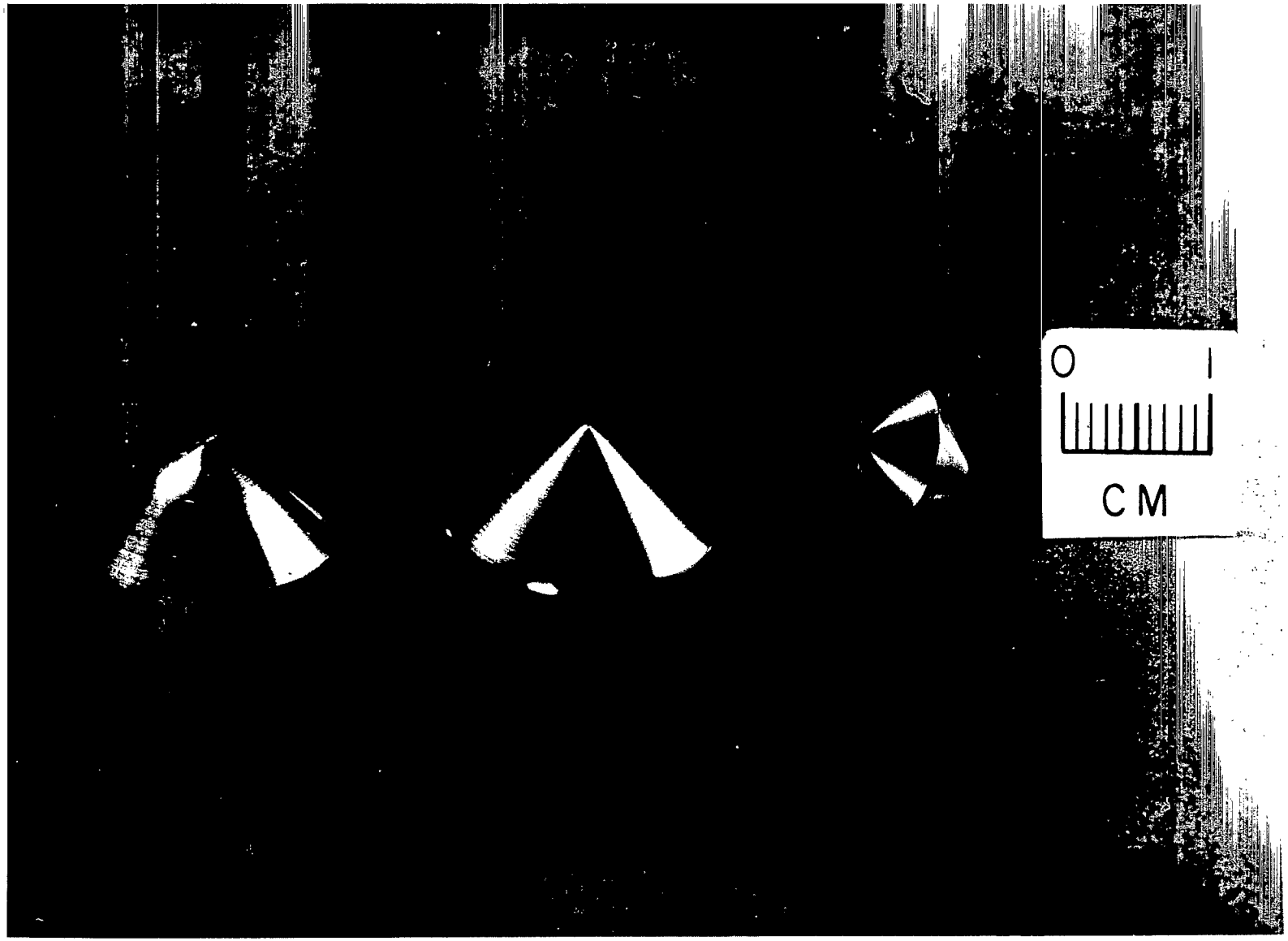

A-42007

(b) High drag bodies.

Figure 3.- Continued.

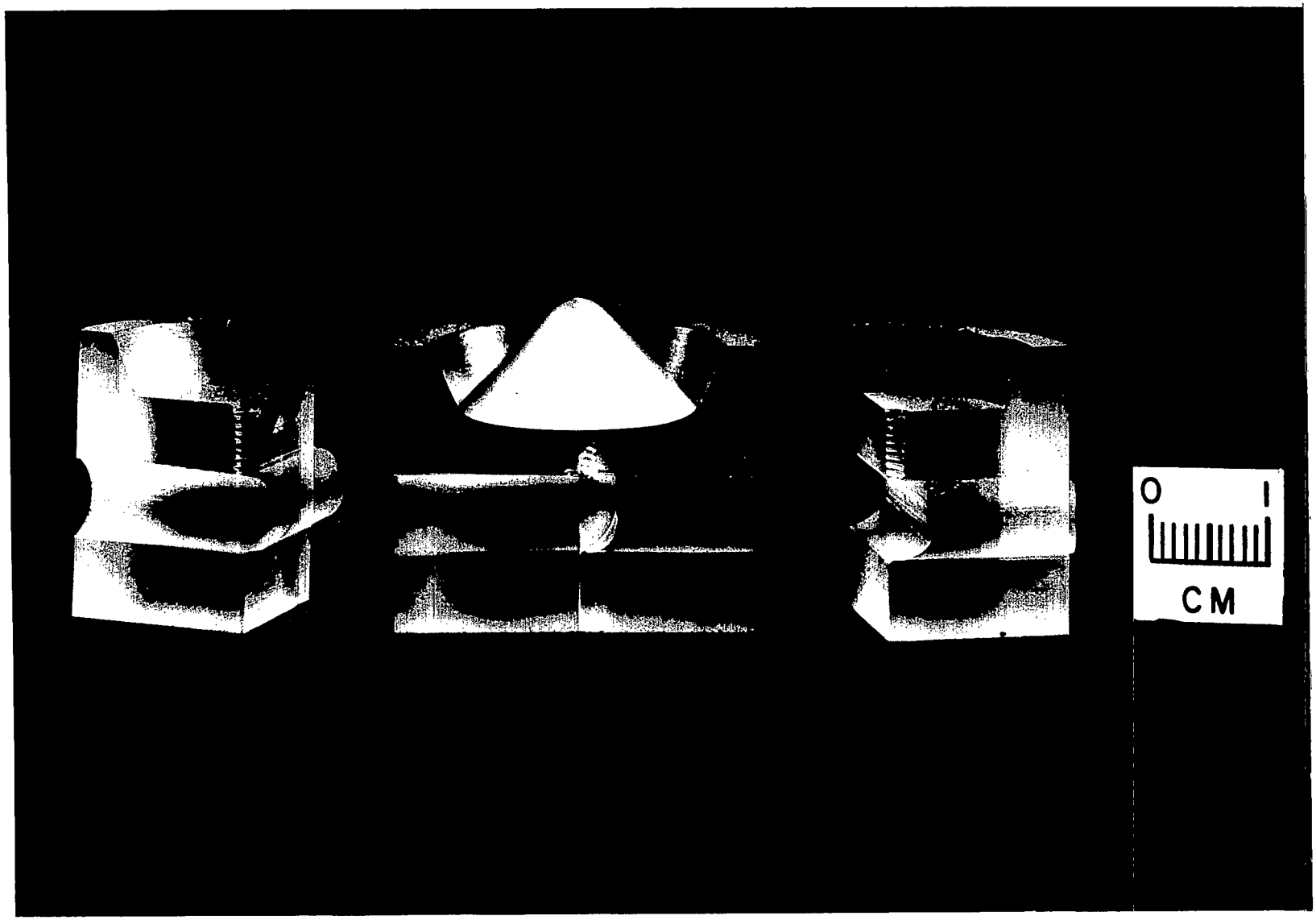

A-36132

(c) Model A and sabot.

Figure 3.- Continued.

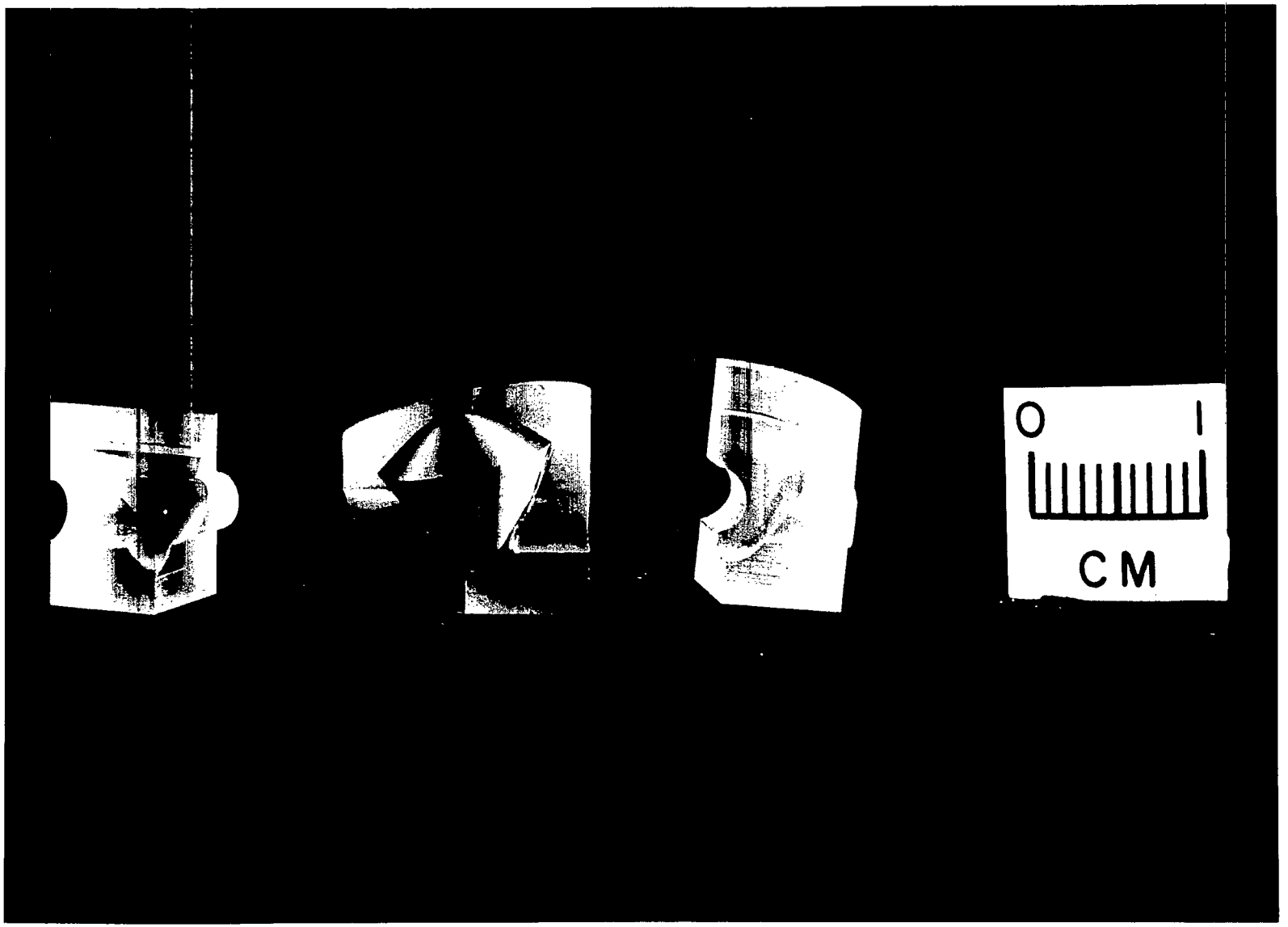

A-36130

(d) Model F and 10° canted sabot.

Figure 3.- Concluded.

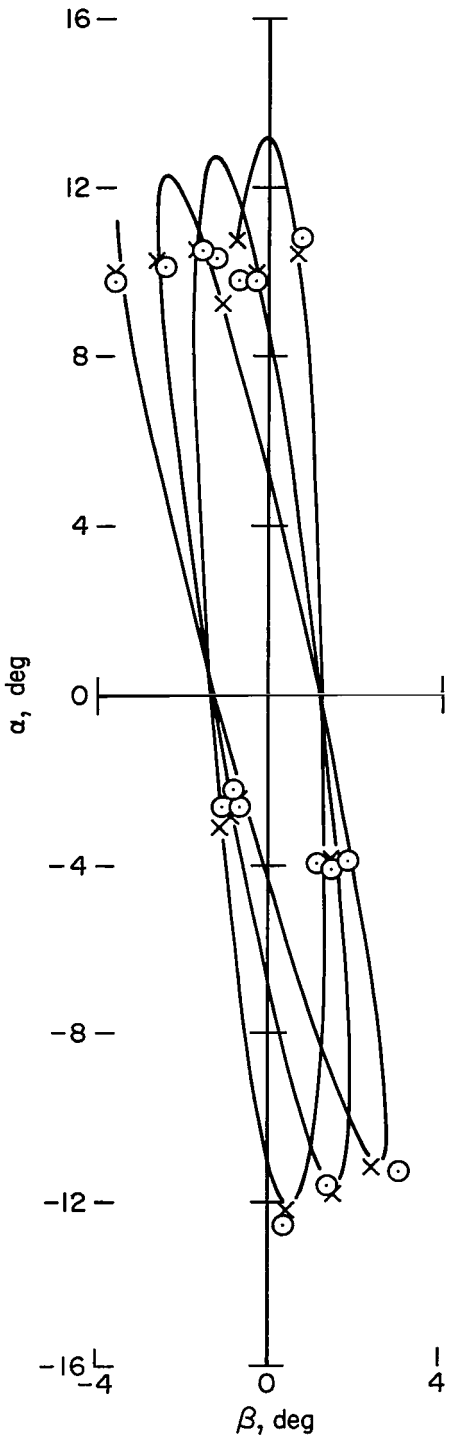

(a) Model B.

Figure 4.- Typical pitching and yawing motions produced by the model.

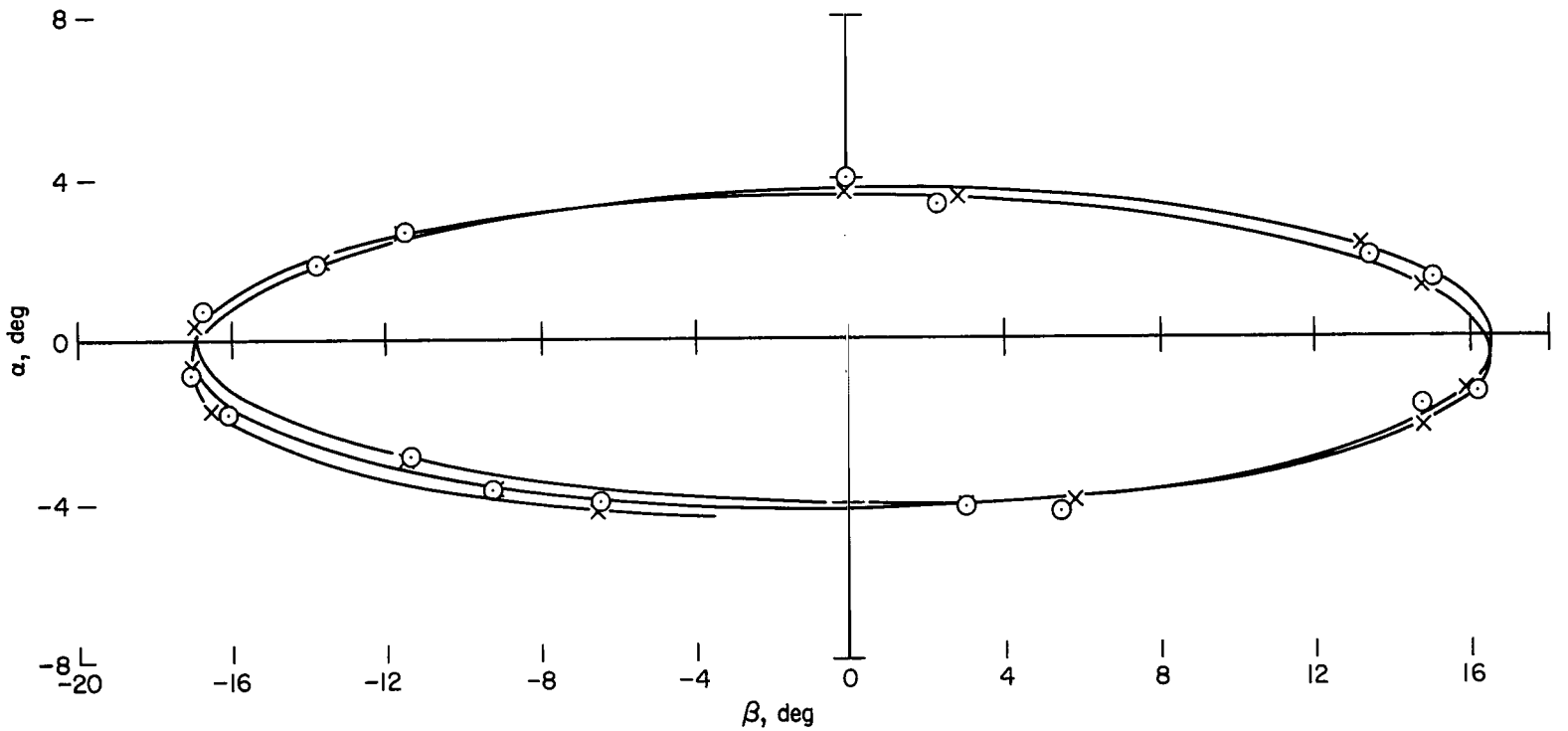

(b) Model D.

Figure 4.- Concluded.

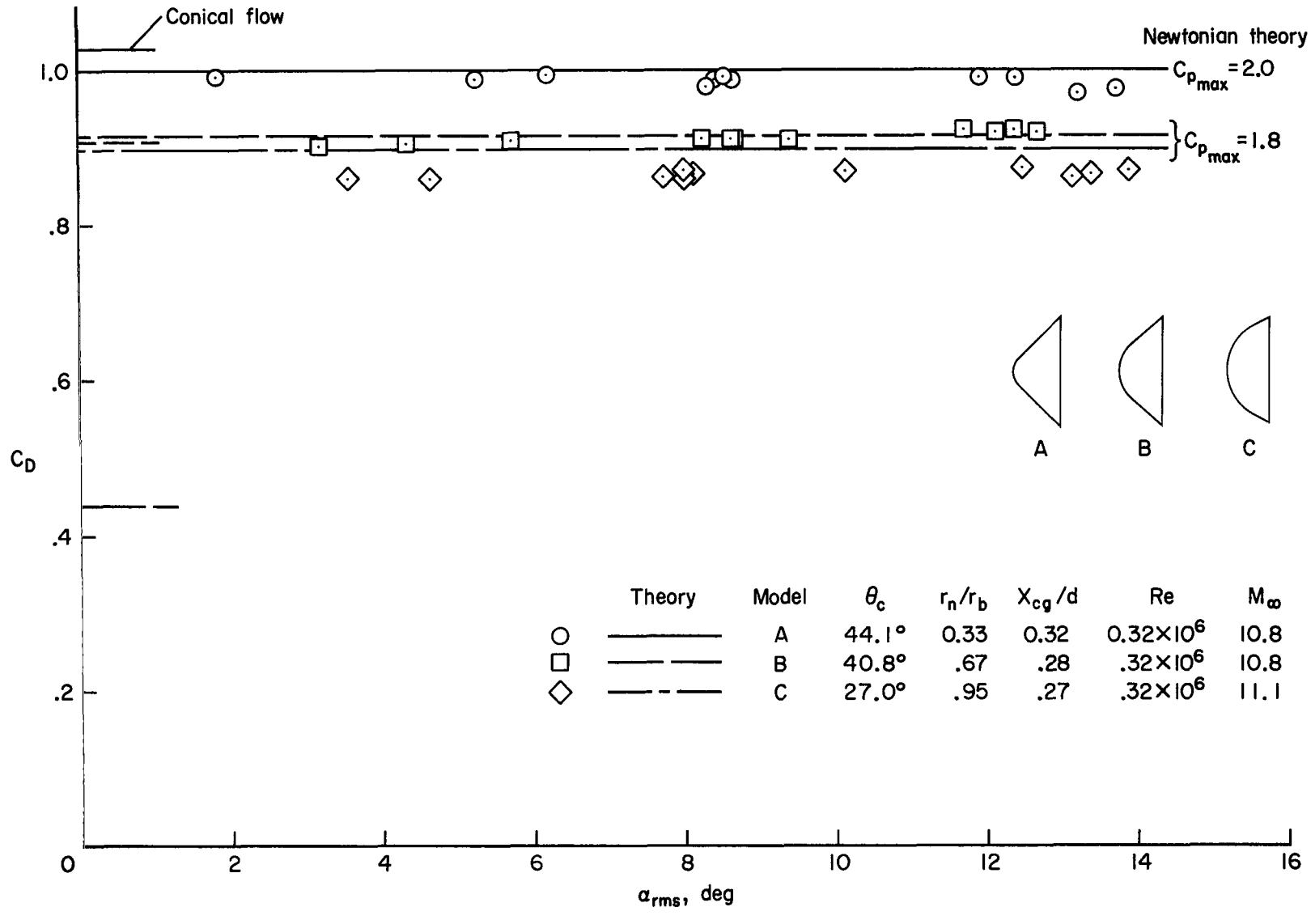

Figure 5.- Variation of drag coefficient with angle of attack for models A, B, and C.

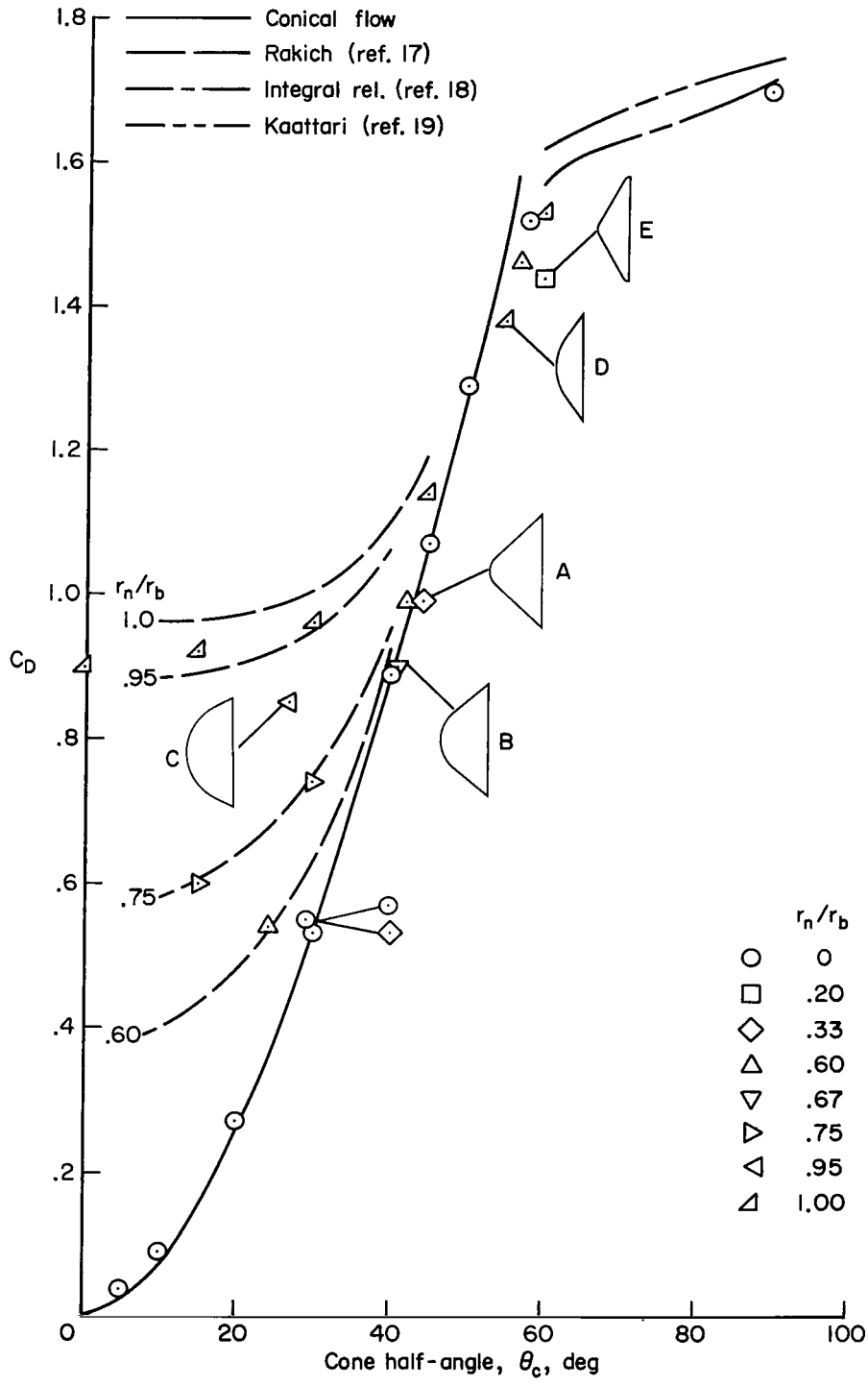

Figure 6.- Variation of the drag coefficient of spherically blunted cones as a function of cone half-angle and nose bluntness.

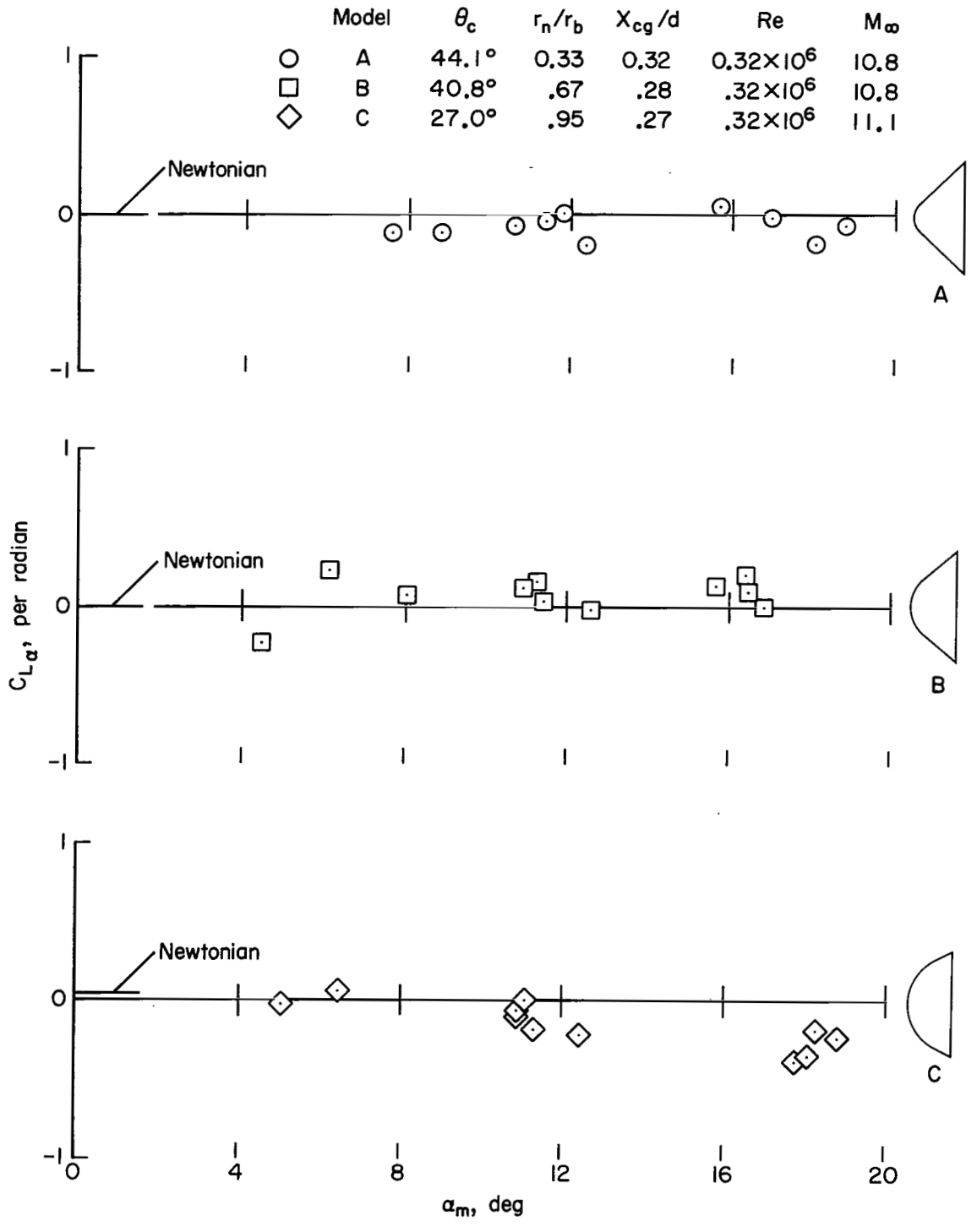

Figure 7.- Variation of the lift-curve slope $\left(C_{L_\alpha}\right)$ with pitch amplitude for models A, B, and C.

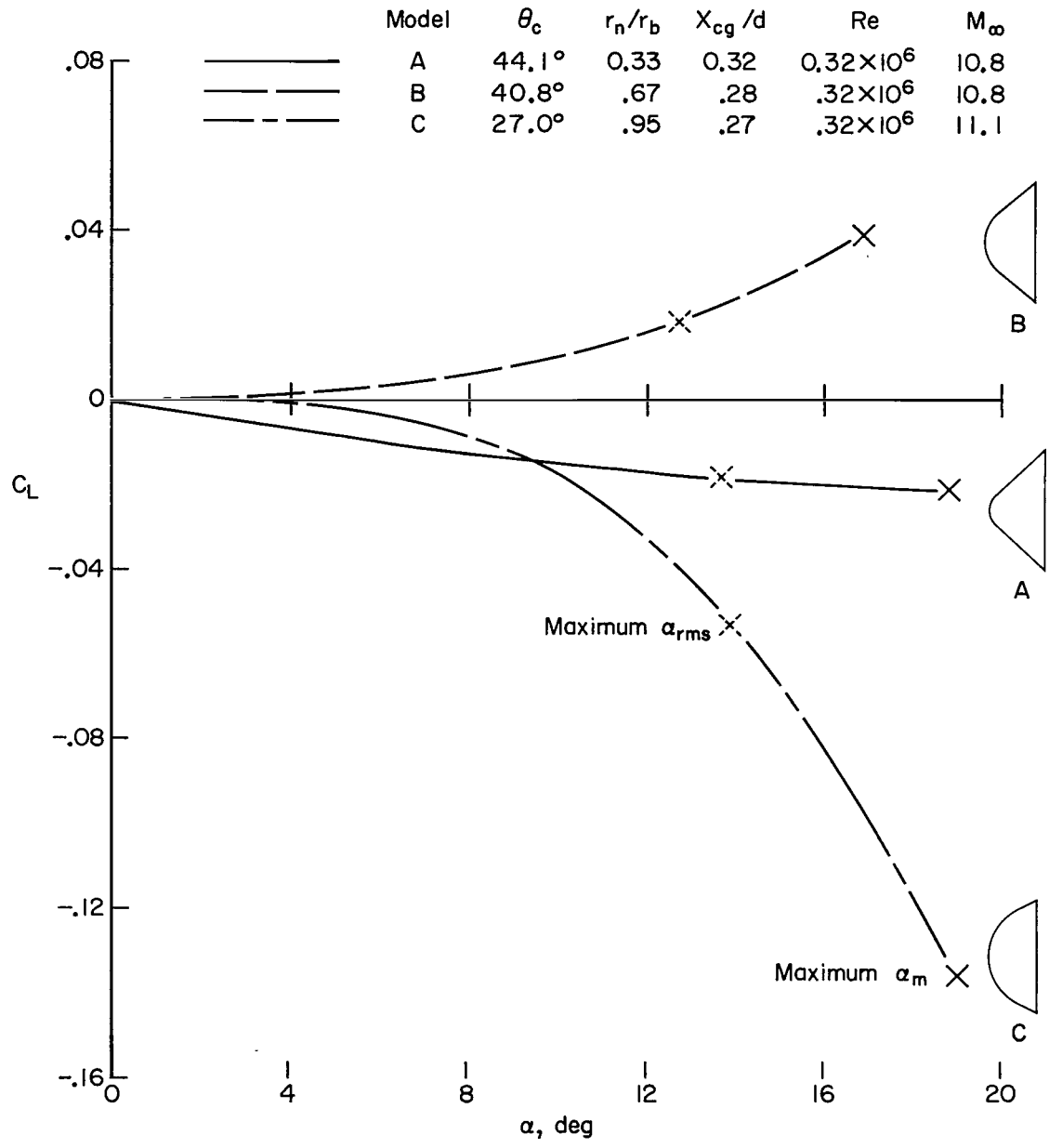

Figure 8.- Variation of lift coefficient with angle of attack for models A, B, and C.

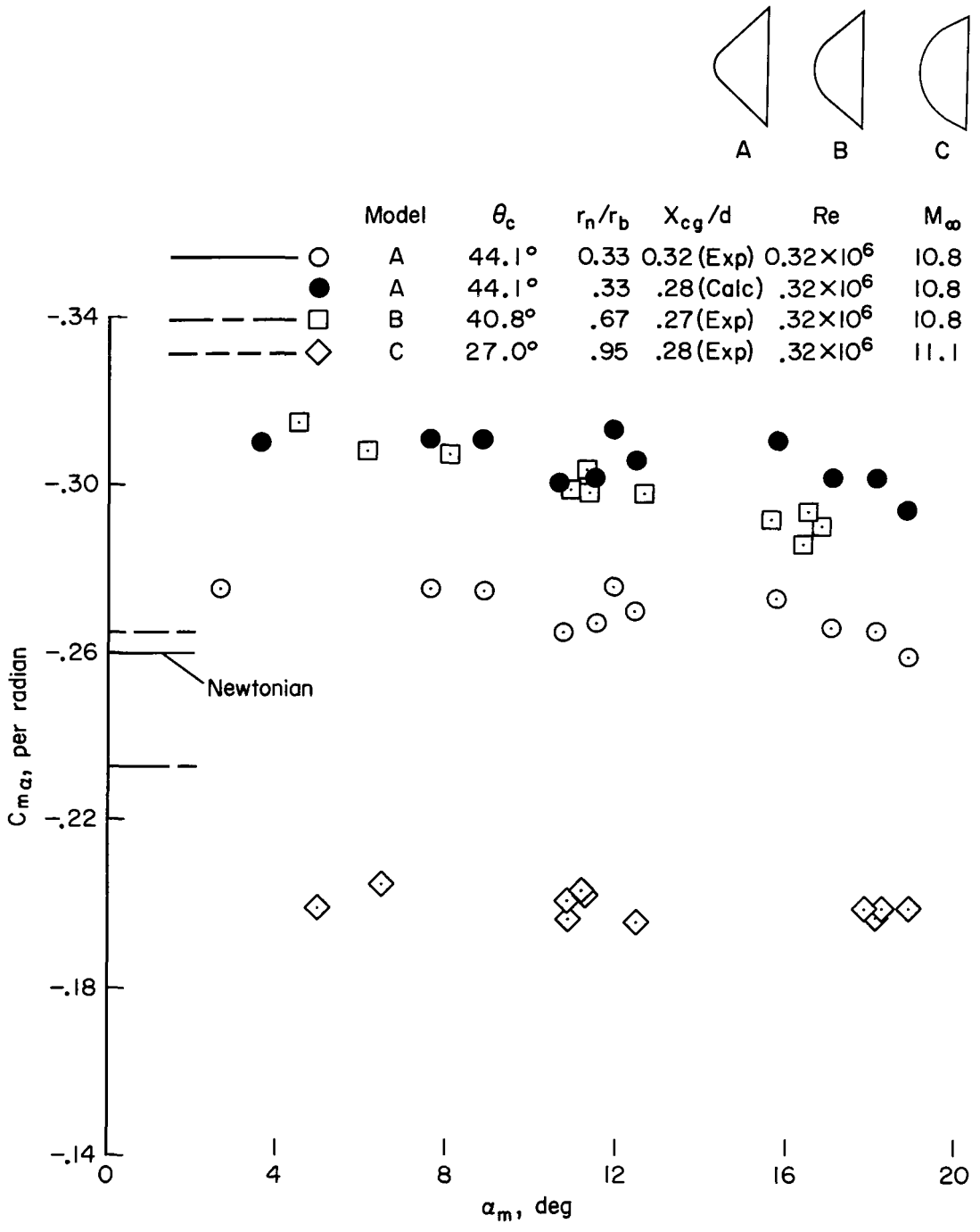

Figure 9.- Variation of the static stability $\left(C_{m_\alpha}\right)$ with pitching amplitude for models A, B, and C.

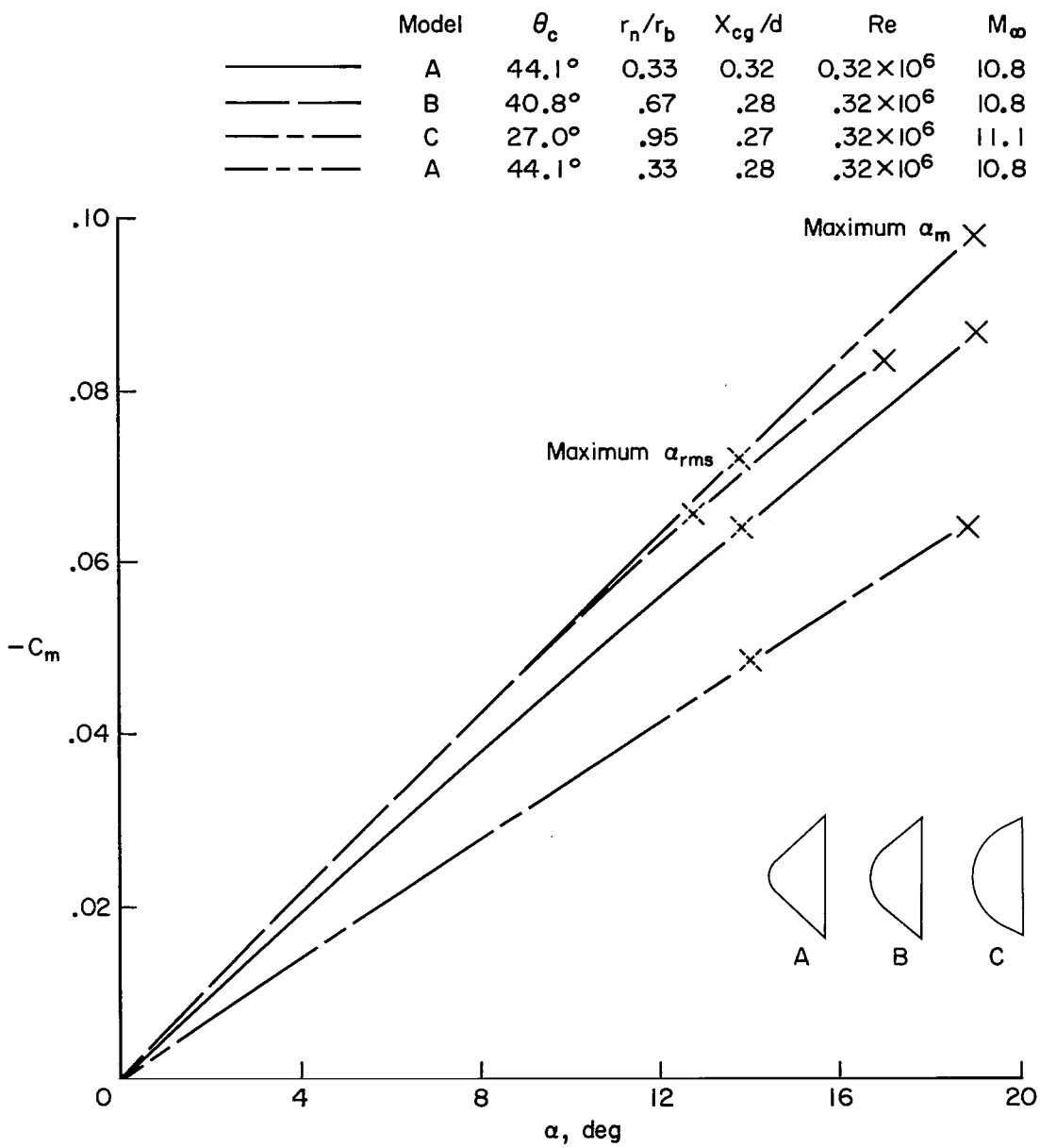

Figure 10.- Variation of the pitching-moment coefficient with angle of attack for models A, B, and C.

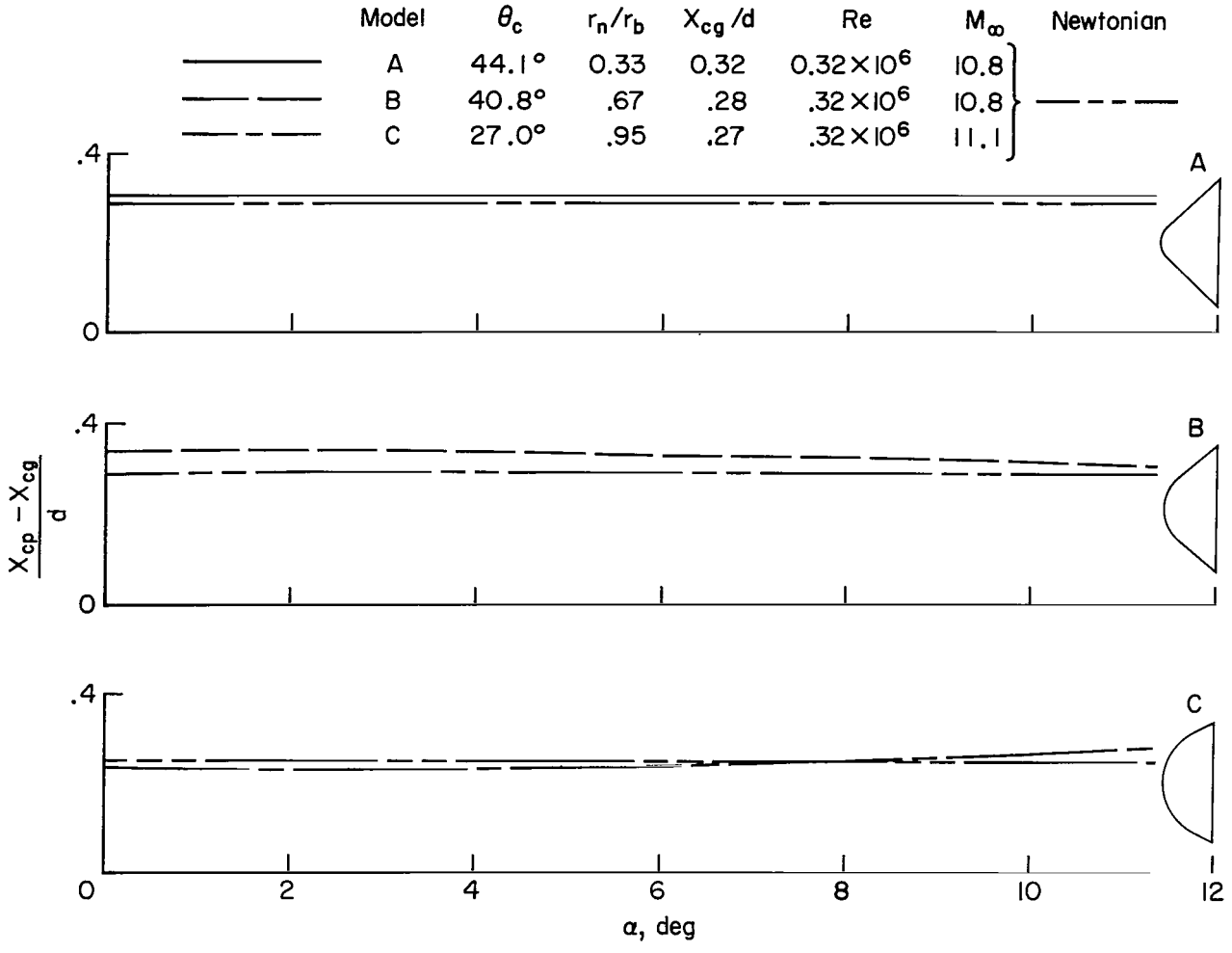

Figure 11.- Variation of the static margin with angle of attack, referred to the homogeneous center of gravity, for models A, B, and C.

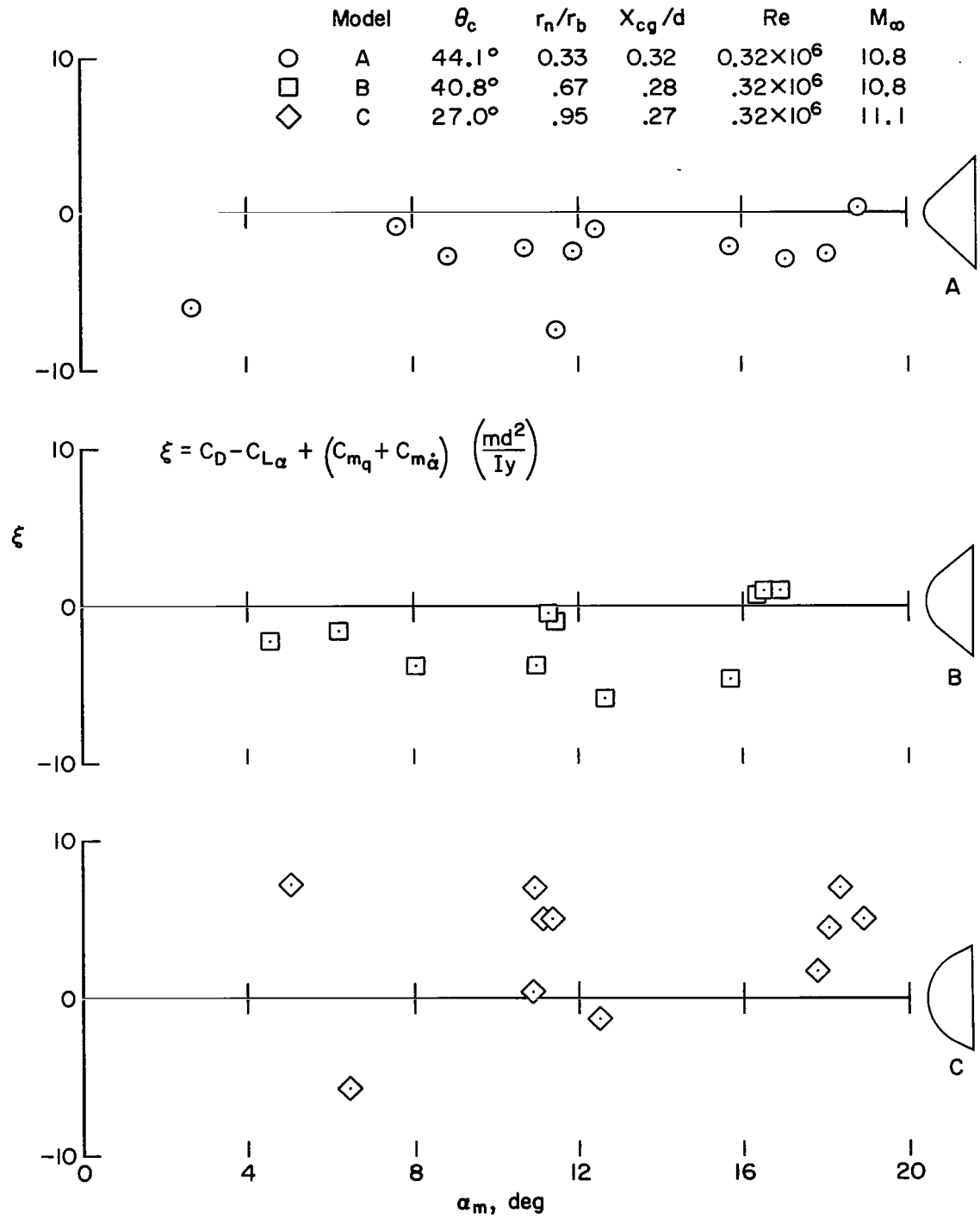

Figure 12.- Variation of the damping parameter (ξ) with pitch amplitude for models A, B, and C.

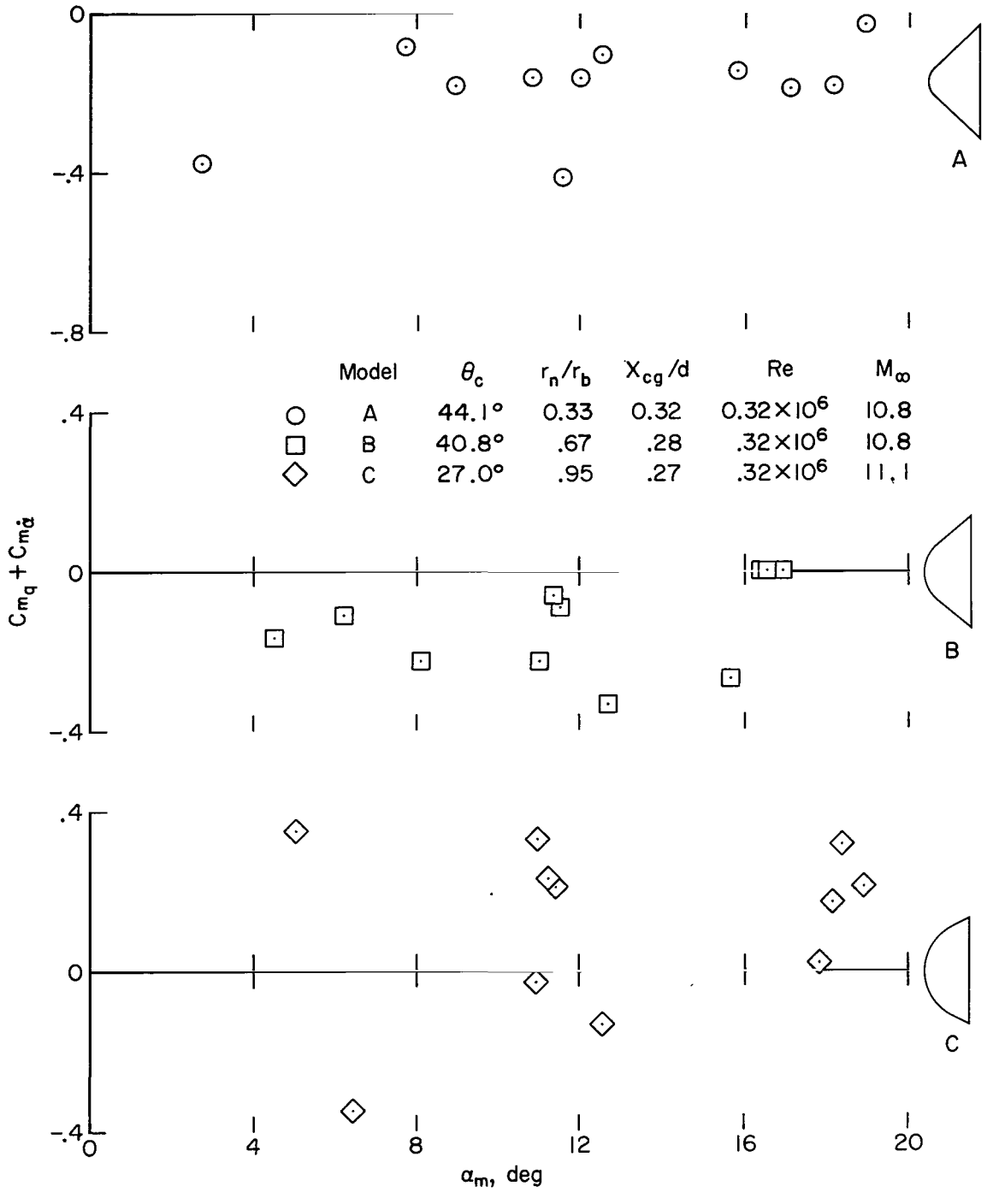

Figure 13.- Variation of the dynamic stability $\left(C_{m_q} + C_{m_{\dot{\alpha}}}\right)$ with pitch amplitude for models A, B, and C.

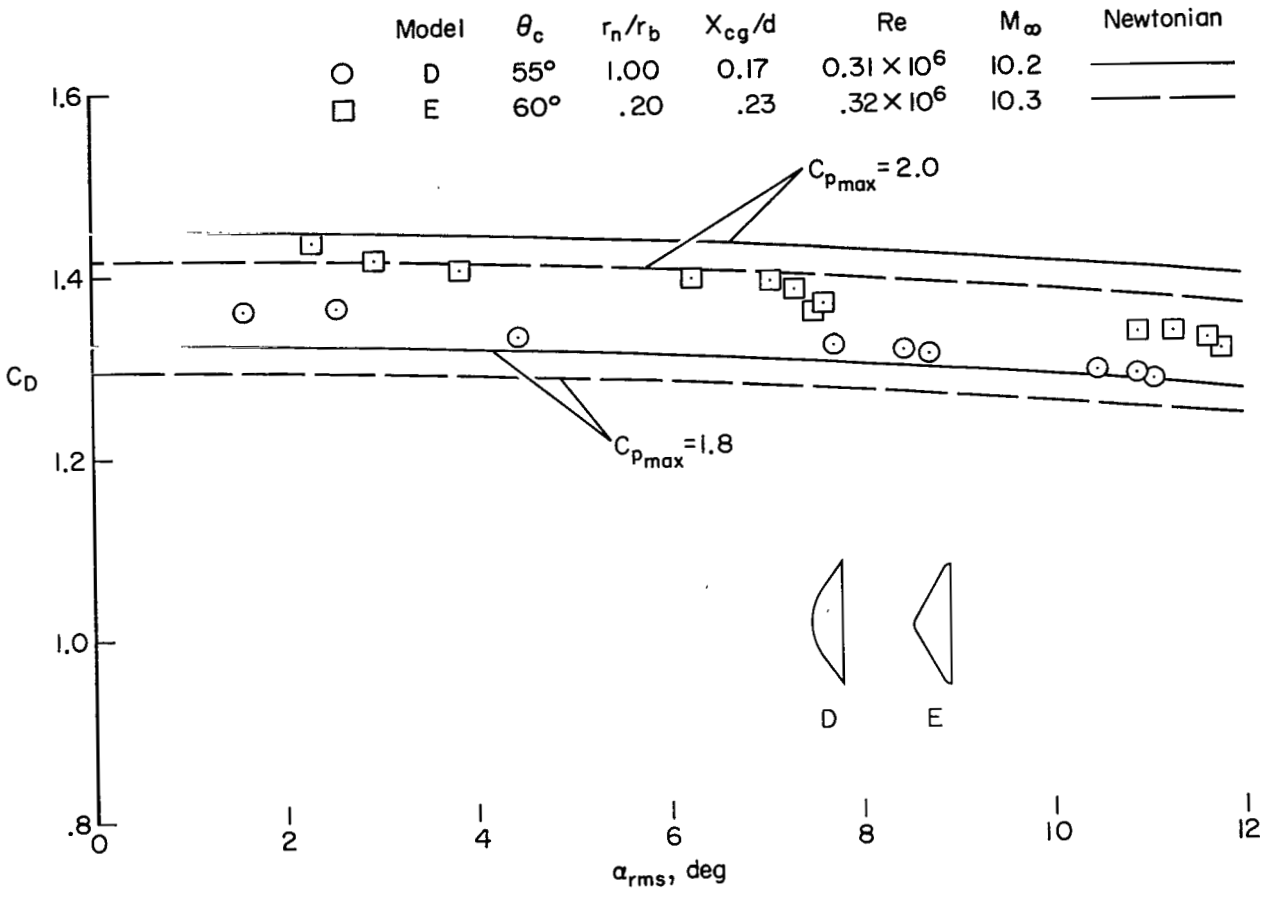

Figure 14.- Variation of the drag coefficient with angle of attack for models D and E.

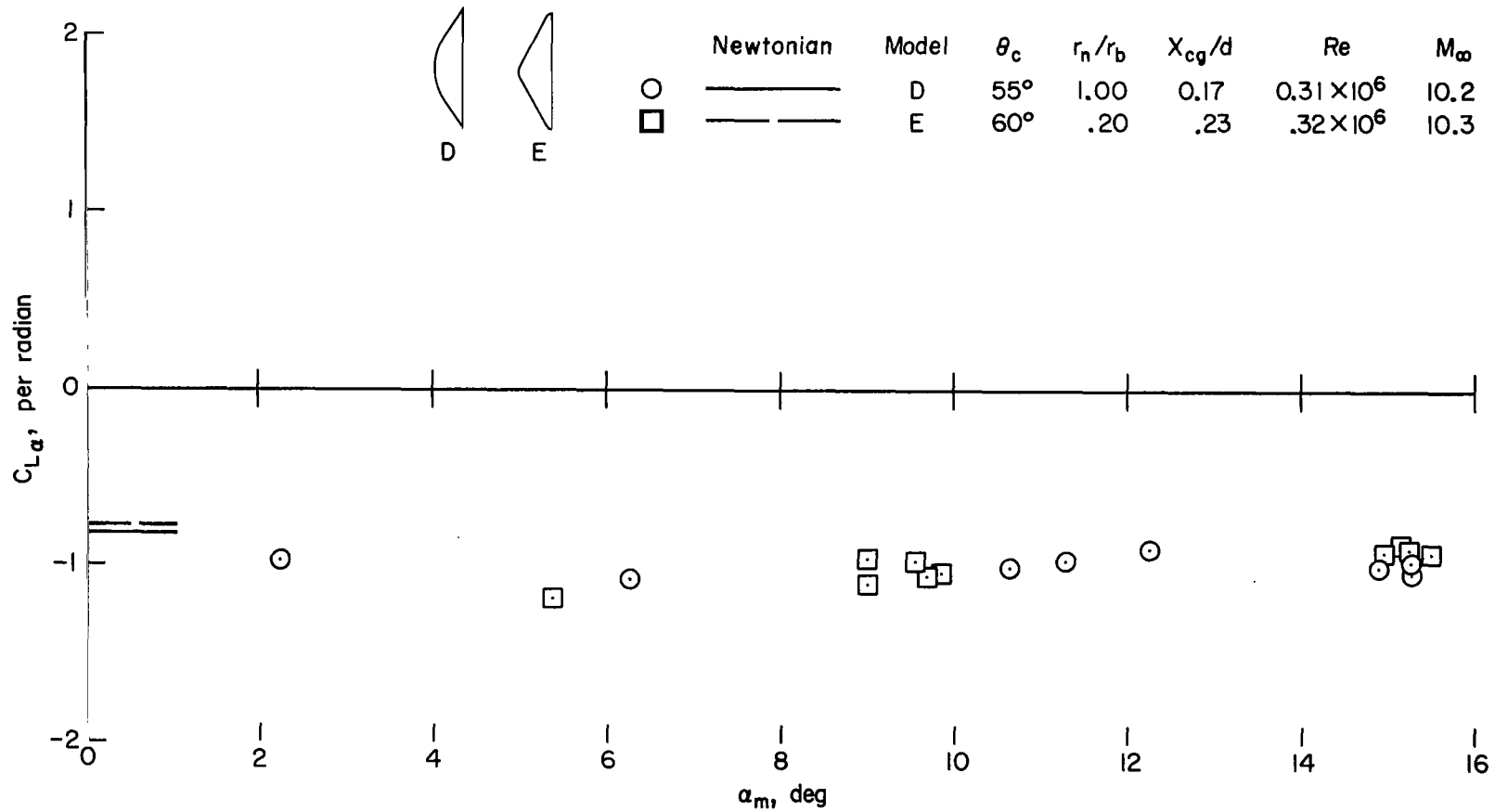

Figure 15.- Variation of the lift-curve slope $\left(C_{L_\alpha}\right)$ with pitch amplitude for models D and E.

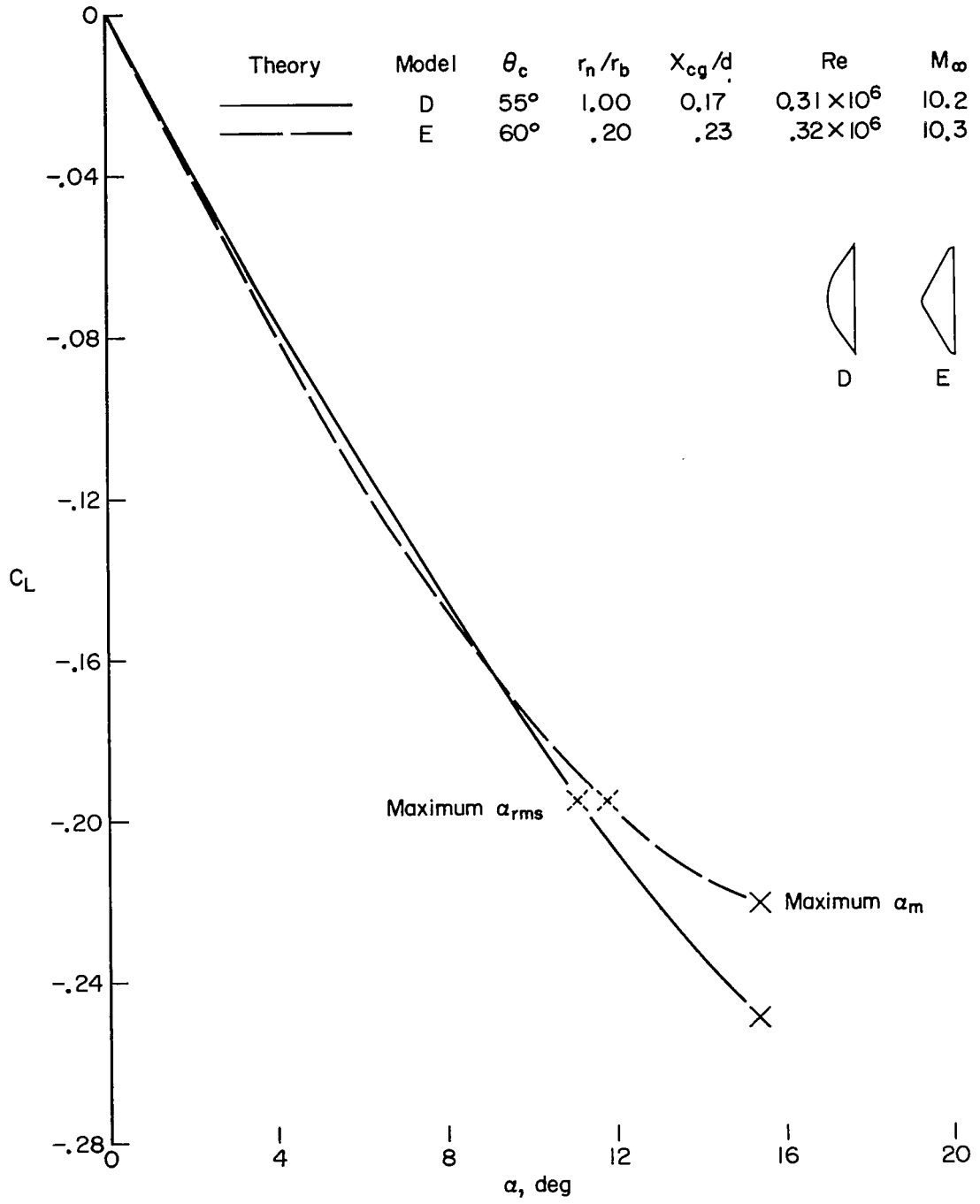

Figure 16.- Variation of lift coefficient with angle of attack for models D and E.

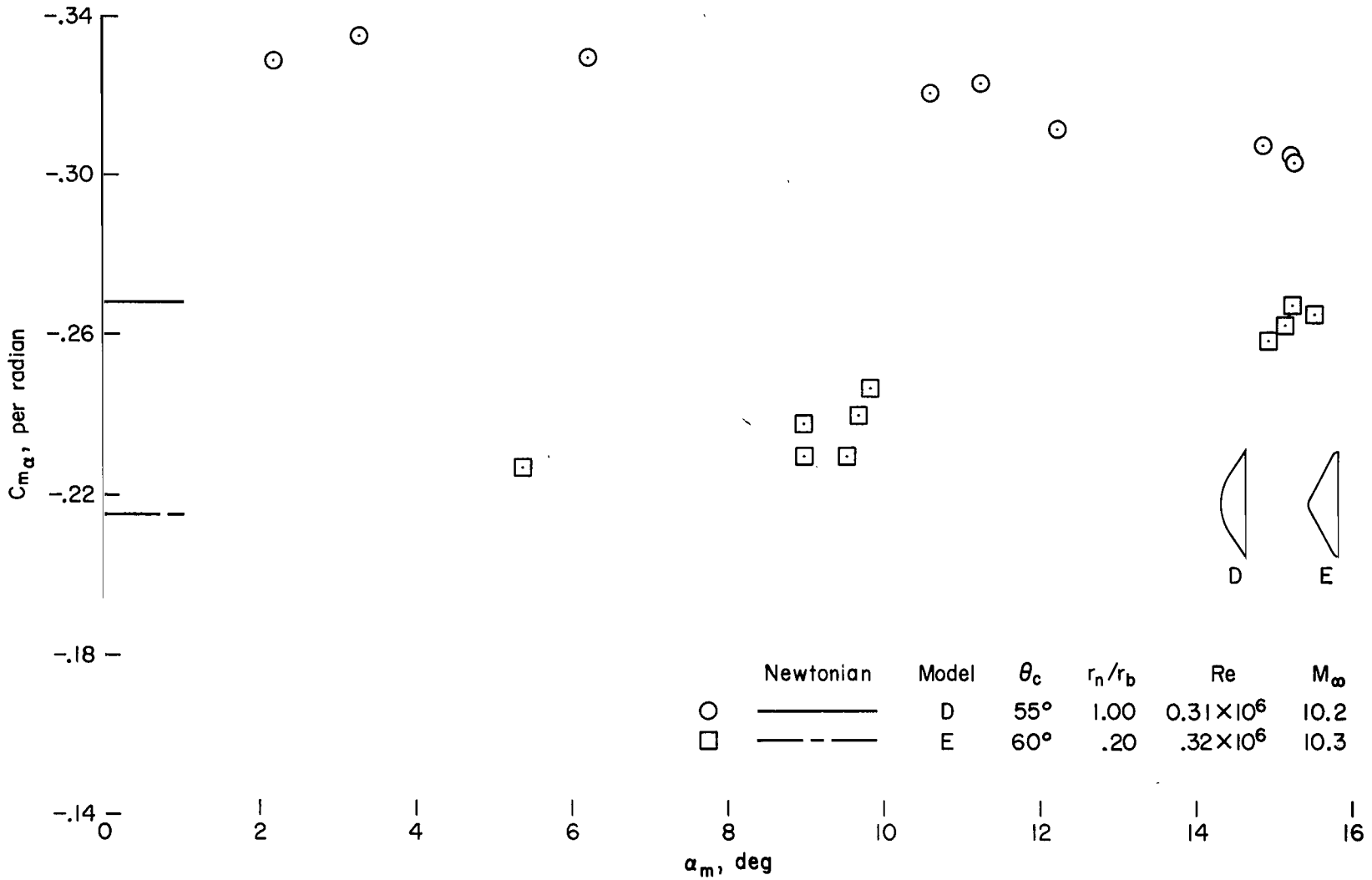

Figure 17.- Variation of the static stability $\left(C_{m_\alpha}\right)$ with pitch amplitude for models D and E, about a moment center at the nose.

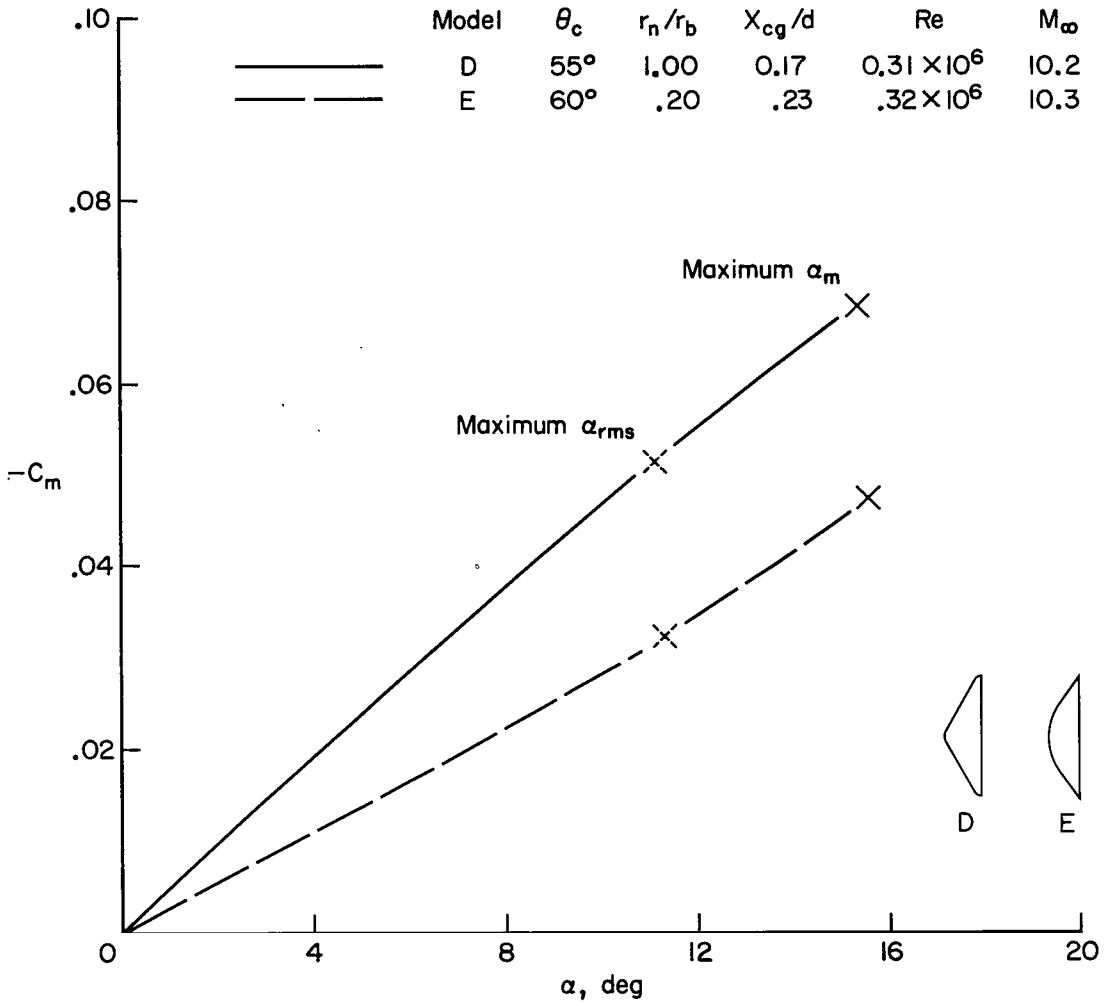

Figure 18.- **Variation of the** pitching-moment **coefficient with** angle of **attack for models** D and E.

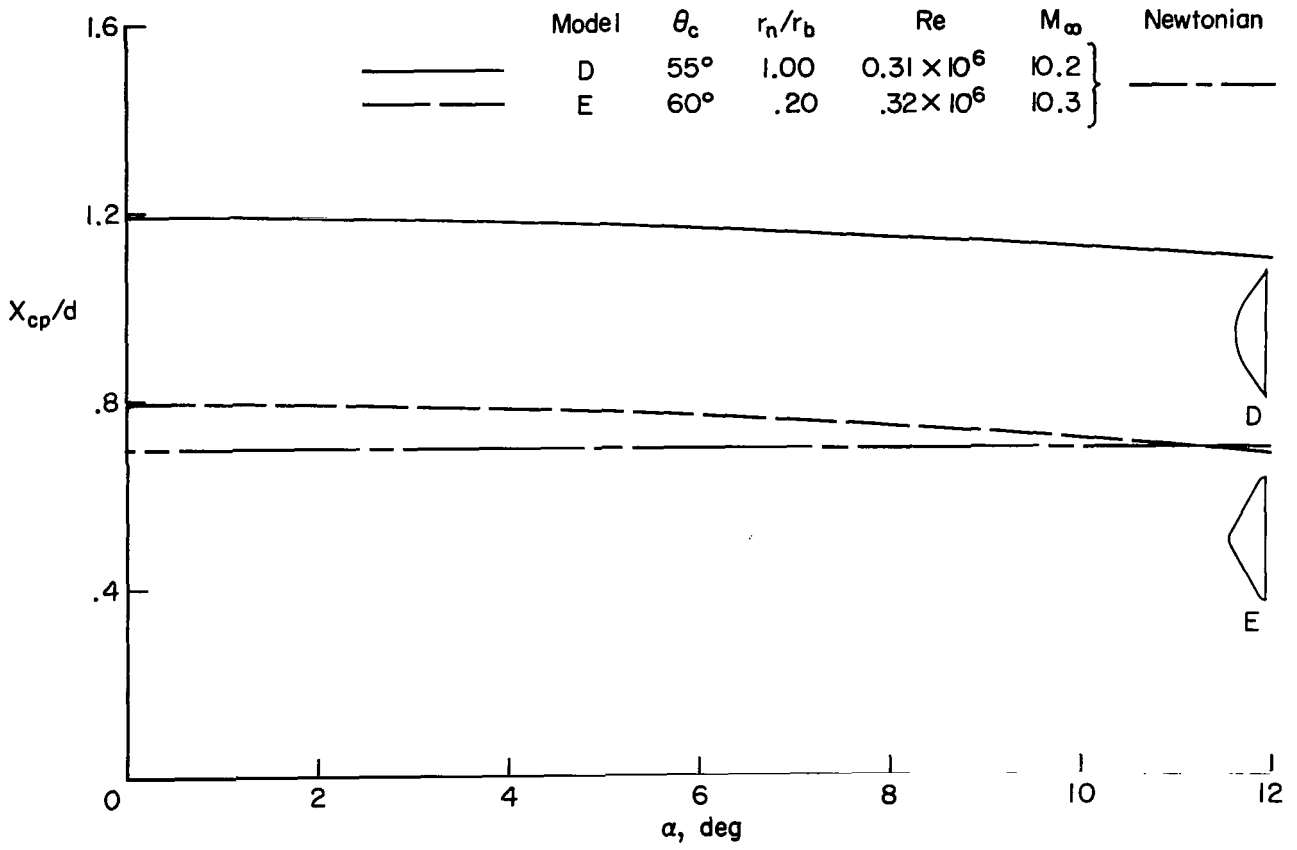

Figure 19.- Variation of the center of pressure with angle of attack for models D and E.

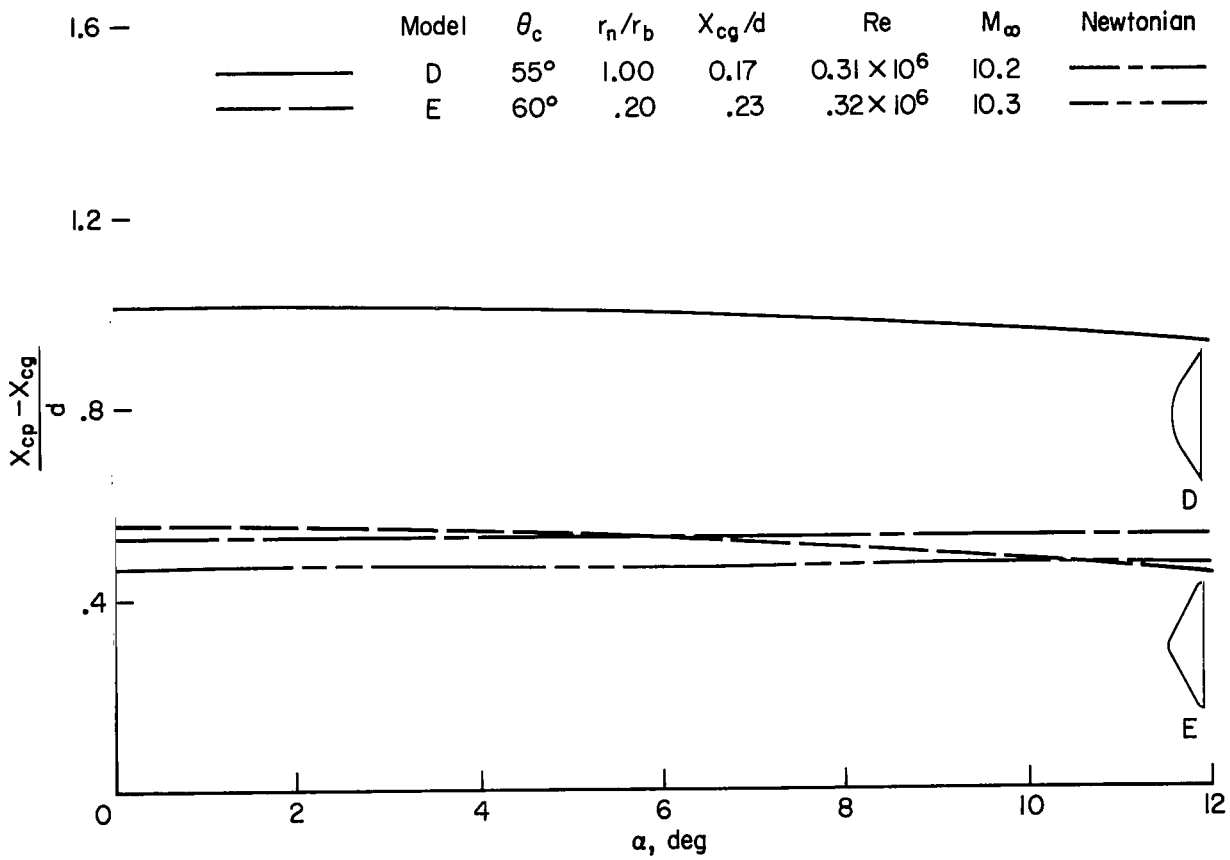

Figure 20.- Variation of the static margin with angle of attack, referred to the homogeneous center of gravity, for models D and E.

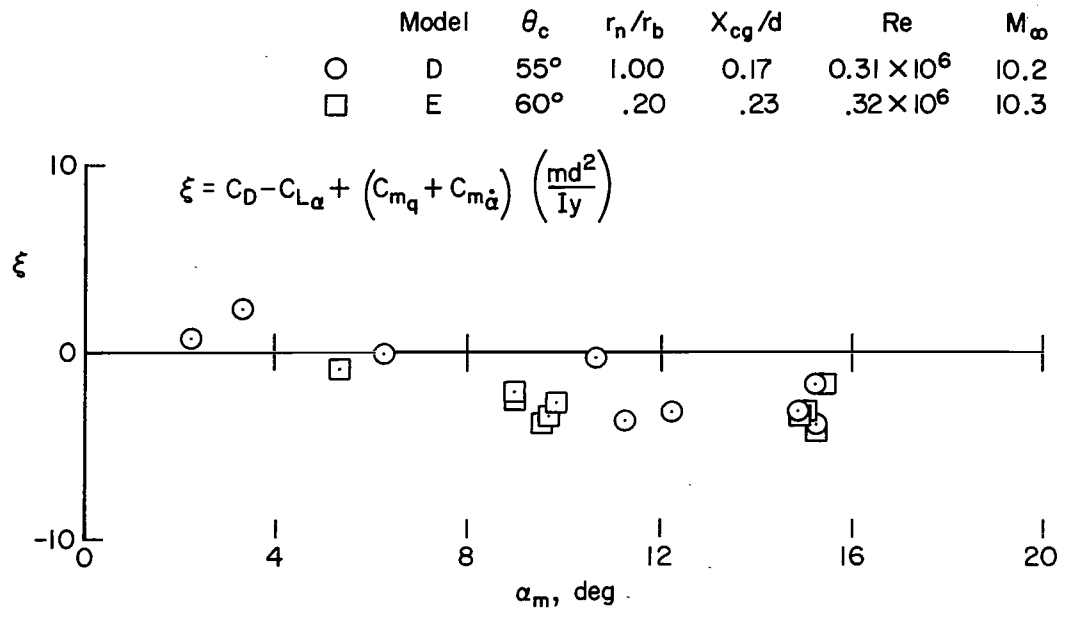

Figure 21.- Variation of the damping parameter (ξ) with pitch amplitude for models D and E.

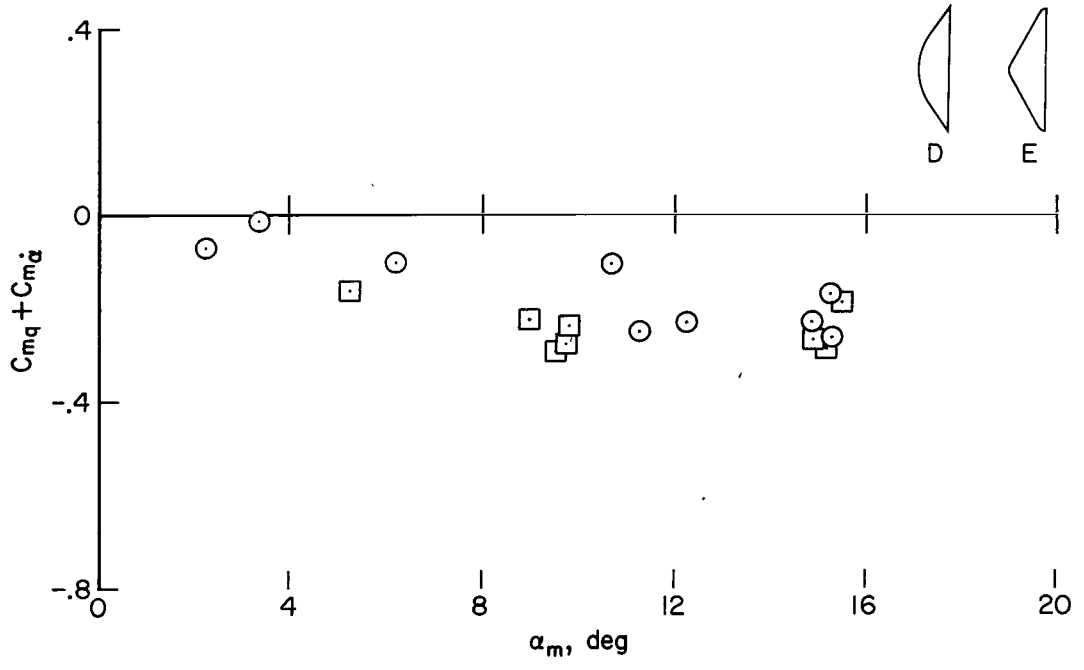

Figure 22.- Variation of the dynamic stability $\left(C_{m_q} + C_{m_{\dot{\alpha}}}\right)$ with pitch amplitude for models D and E.

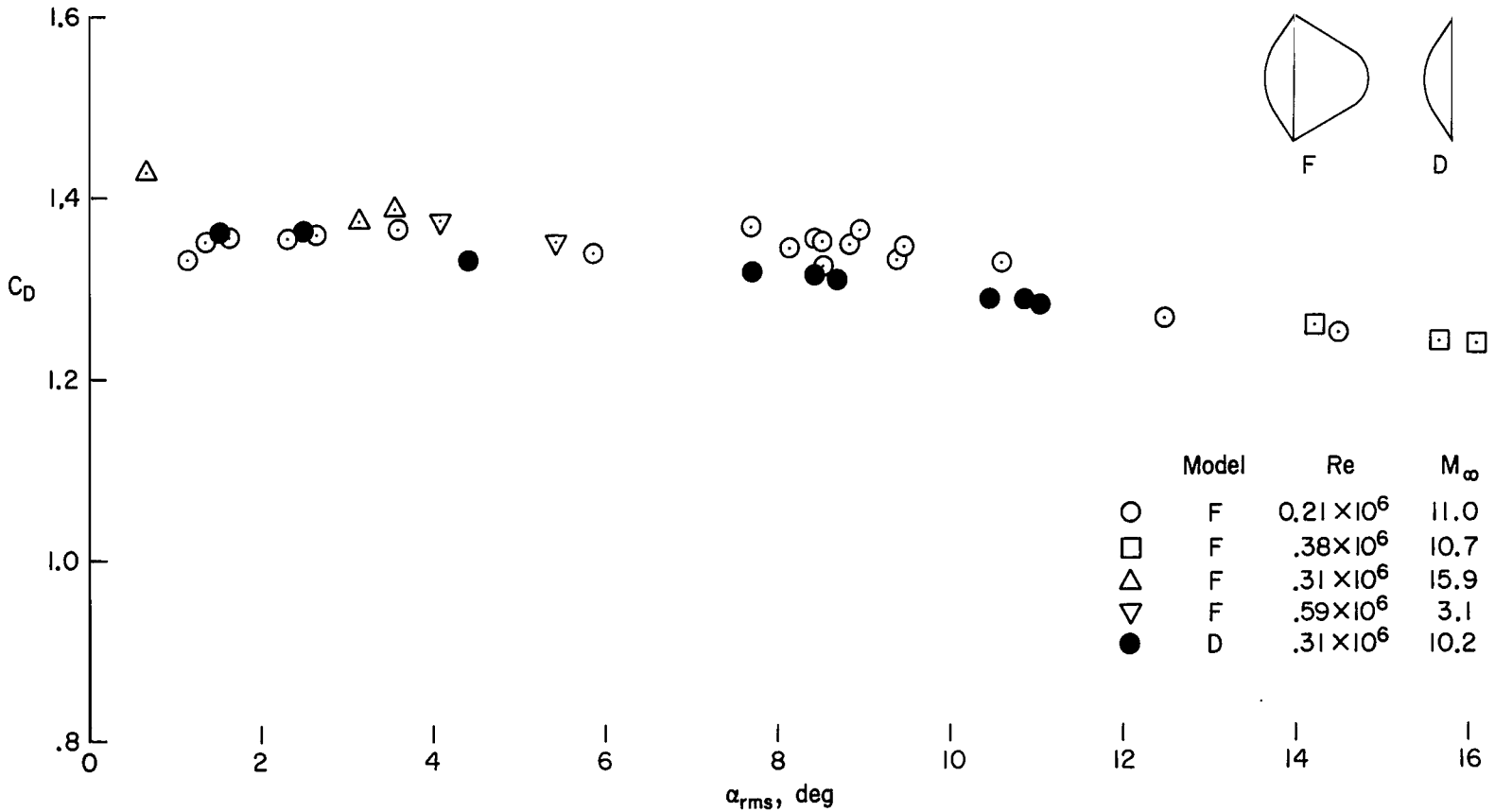

Figure 23.- Effect of afterbody shape on the drag coefficient of a 55° half-angle blunt cone; models D and F.

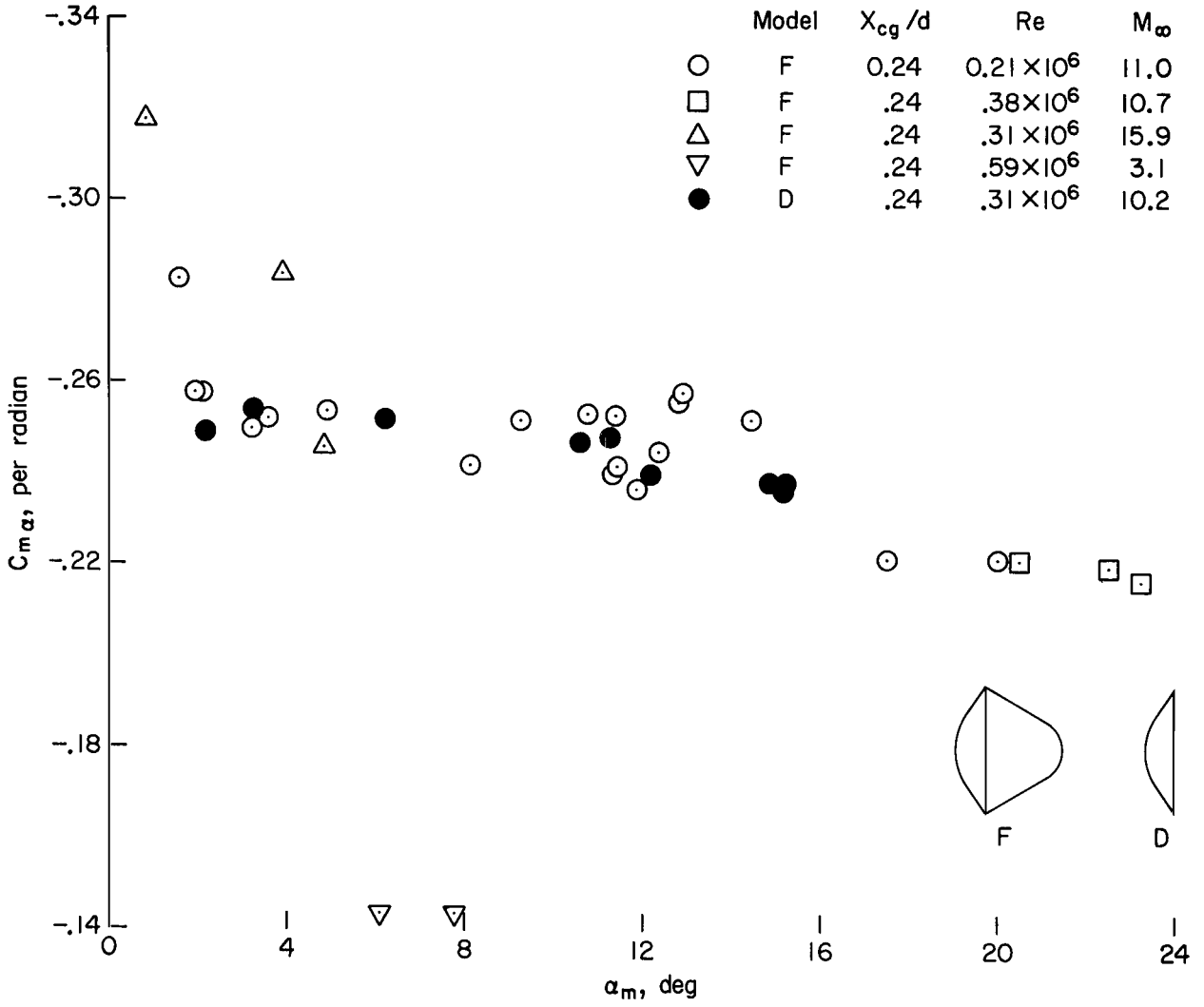

Figure 24.- Effect of afterbody shape on the static stability $\left(C_{m_\alpha}\right)$ of a 55° half-angle blunt cone; models D and F.

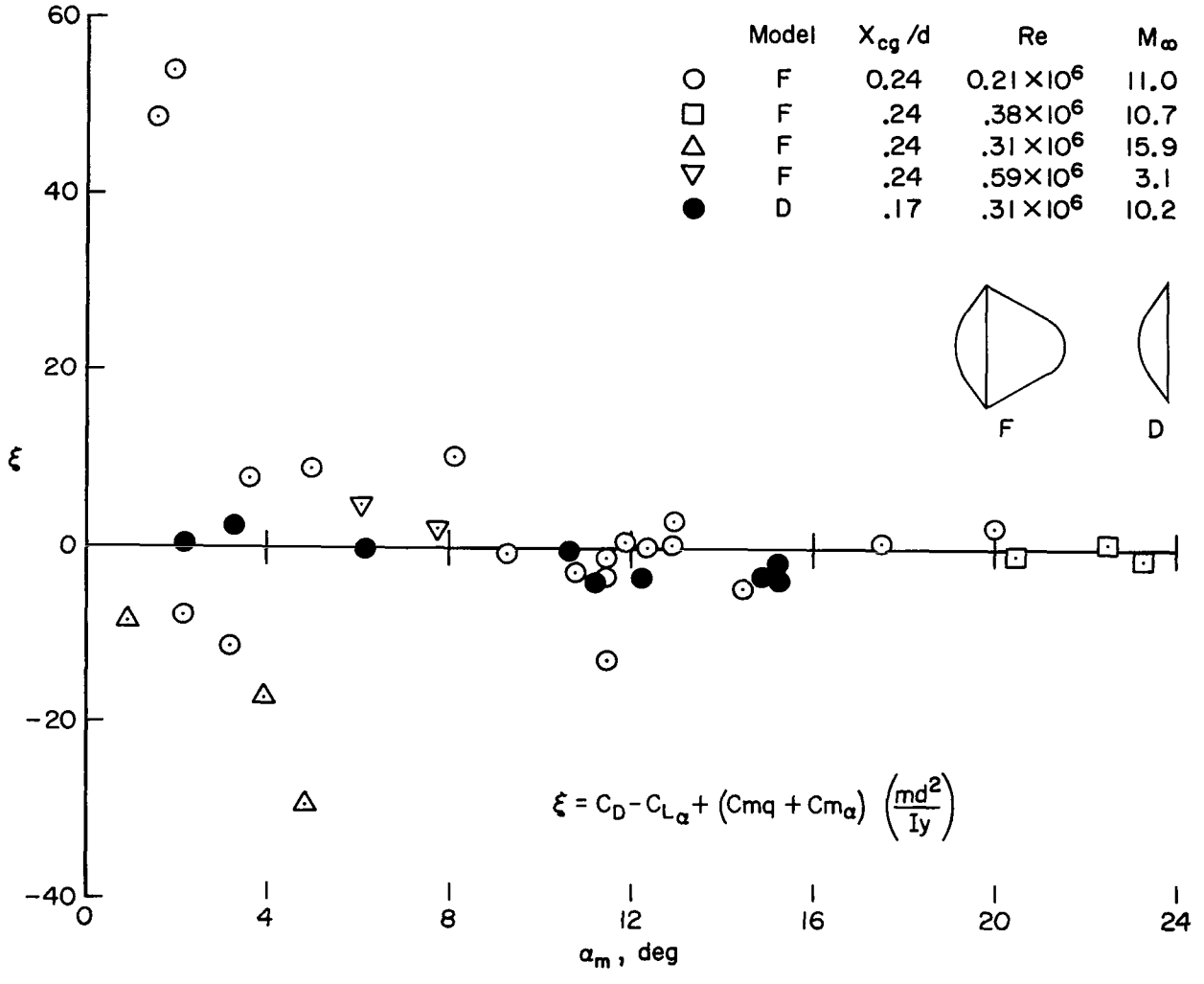

Figure 25.- Effect of afterbody shape on the damping parameter (ξ) of a 55° half-angle blunt cone; models D and F.

NATIONAL AERONAUTICS AND SPACE ADMINISTRATION
WASHINGTON, D. C. 20546

OFFICIAL BUSINESS

FIRST CLASS MAIL

POSTAGE AND FEES PAID
NATIONAL AERONAUTICS AND
SPACE ADMINISTRATION

"The aeronautical and space activities of the United States shall be conducted so as to contribute . . . to the expansion of human knowledge of phenomena in the atmosphere and space. The Administration shall provide for the widest practicable and appropriate dissemination of information concerning its activities and the results thereof."

NATIONAL AERONAUTICS AND SPACE ACT OF 1958

NASA SCIENTIFIC AND TECHNICAL PUBLICATIONS

TECHNICAL REPORTS: Scientific and technical information considered important, complete, and a lasting contribution to existing knowledge.

TECHNICAL NOTES: Information less broad in scope but nevertheless of importance as a contribution to existing knowledge.

TECHNICAL MEMORANDUMS: Information receiving limited distribution because of preliminary data, security classification, or other reasons.

CONTRACTOR REPORTS: Scientific and technical information generated under a NASA contract or grant and considered an important contribution to existing knowledge.

TECHNICAL TRANSLATIONS: Information published in a foreign language considered to merit NASA distribution in English.

SPECIAL PUBLICATIONS: Information derived from or of value to NASA activities. Publications include conference proceedings, monographs, data compilations, handbooks, sourcebooks, and special bibliographies.

TECHNOLOGY UTILIZATION PUBLICATIONS: Information on technology used by NASA that may be of particular interest in commercial and other non-aerospace applications. Publications include Tech Briefs, Technology Utilization Reports and Notes, and Technology Surveys.

Details on the availability of these publications may be obtained from:

SCIENTIFIC AND TECHNICAL INFORMATION DIVISION

NATIONAL AERONAUTICS AND SPACE ADMINISTRATION

Washington, D.C. 20546